Inorganic Chemistry
Article

Inorg. Chem. **2010**, *49*, 10041–10056 **10041**
DOI: 10.1021/ic101344t

Structure and Ultrafast Dynamics of the Charge-Transfer Excited State and Redox Activity of the Ground State of Mono- and Binuclear Platinum(II) Diimine Catecholate and Bis-catecholate Complexes: A Transient Absorption, TRIR, DFT, and Electrochemical Study

Jonathan Best,[†] Igor V. Sazanovich,[†] Harry Adams,[†] Robert D. Bennett,[†] E. Stephen Davies,[‡] Anthony J. H. M. Meijer,[†] Michael Towrie,[§] Sergei A. Tikhomirov,[⊥] Oleg V. Bouganov,[⊥] Michael D. Ward,*[,†] and Julia A. Weinstein*[,†]

[†]*Department of Chemistry, University of Sheffield, Sheffield S3 7HF, U.K.,* [‡]*School of Chemistry, University of Nottingham, Nottingham NG7 2RD, U.K.,* [§]*Central Laser Facility, Rutherford Appleton Laboratory, Harwell Science and Innovation Campus, STFC, Chilton, Oxfordshire OX11 0QX, U.K., and* [⊥]*B. I. Stepanov Institute of Physics, Minsk, Belarus*

Received July 6, 2010

A series of mononuclear complexes of the type [Pt(Bu_2cat)(4,4′-R_2-bipy)] [where Bu_2cat is the dianion of 3,5-$^tBu_2$-catechol and R = H, ^{t}Bu, or C(O)NEt_2] and analogous dinuclear complexes based on the "back-to-back" bis-catechol ligand 3,3′,4,4′-tetrahydroxybiphenyl have been studied in detail in both their ground and excited states by a range of physical methods including electrochemistry, UV/vis/near-IR, IR, and electron paramagnetic resonance spectroelectrochemistry, and time-resolved IR (TRIR) and transient absorption (TA) spectroscopy. Density functional theory calculations have been performed to support these studies, which provide a detailed picture of the ground- and excited-state electronic structures, and excited-state dynamics, of these complexes. Notable observations include the following: (i) for the first time, the lowest-energy catecholate → bipyridine (bpy) ligand-to-ligand charge-transfer (LL′CT) excited states of these chromophores have been studied by TRIR spectroscopy, showing a range of transient bands associated with the bpy radical anion and semiquinone species, and back-electron-transfer occurring in hundreds of picoseconds; (ii) strong electronic coupling between the two catecholate units in the bridging ligand of the dinuclear complexes results in a delocalized, planar (class 3) "mixed-valence" catecholate^{2-}/semiquinone$^{\bullet-}$ state formed by one-electron oxidation of the bridging ligand; (iii) in the LL′CT excited state of the dinuclear complexes, the bridging ligand is symmetrical and delocalized, whereas the bpy radical anion is localized at one terminus of the complex. This study is the first example of an investigation of excited-state behavior in platinum(II) catecholate complexes, performed with the use of picosecond TRIR and femtosecond TA spectroscopy.

Introduction

Ligands of the dioxolene family (the catecholate, semiquinone, and quinone series) have been of particular interest in coordination chemistry for several reasons. Their often reversible redox interconversions provide complexes with rich electrochemical behavior, and when combined with metal atoms that are also, in principle, redox-active, an extensive series of complexes displaying "noninnocent" redox behavior in which there is extensive mixing between metal- and ligand-based frontier orbitals have been generated.

The three different redox states of a simple dioxolene ligand generally have distinctly different spectroscopic characteristics with intense charge-transfer bands appearing in different regions of the electronic spectrum as the oxidation state changes.[1−10] For example, catecholate can act as a donor in charge-transfer states such as ligand-to-ligand

*To whom correspondence should be addressed. E-mail: Julia.Weinstein@Sheffield.ac.uk (J.A.W.), M.D.Ward@Sheffield.ac.uk (M.D.W.).

(1) Meacham, A. P.; Druce, K. L.; Bell, Z. R.; Ward, M. D.; Keister, J. B.; Lever, A. B. P. *Inorg. Chem.* **2003**, *42*, 7887–7896.
(2) Garcia-Canadas, J.; Meacham, A. P.; Peter, L. M.; Ward, M. D. *Electrochem. Commun.* **2003**, *5*, 416–420.
(3) Barthram, A. M.; Reeves, Z. R.; Jeffery, J. C.; Ward, M. D. *J. Chem. Soc., Dalton Trans.* **2000**, 3162–3169.
(4) Shukla, A. D.; Whittle, B.; Bajaj, H. C.; Das, A.; Ward, M. D. *Inorg. Chim. Acta* **1999**, *285*, 89–96.
(5) Barthram, A. M.; Cleary, R. L.; Jeffery, J. C.; Couchman, S. M.; Ward, M. D. *Inorg. Chim. Acta* **1998**, *267*, 1–5.
(6) Whittle, B.; Everest, N. S.; Howard, C.; Ward, M. D. *Inorg. Chem.* **1995**, *34*, 2025–2032.
(7) Barthram, A. M.; Ward, M. D. *New J. Chem.* **2000**, *24*, 501–504.
(8) Rice, C. R.; Ward, M. D.; Nazeeruddin, M. K.; Gratzel, M. *New J. Chem.* **2000**, *24*, 651–652.
(9) Joulie, L. F.; Schatz, E.; Ward, M. D.; Weber, F.; Yellowlees, L. J. *J. Chem. Soc., Dalton Trans.* **1994**, 799–804.
(10) Fox, G. A.; Bhattacharya, S.; Pierpont, C. G. *Inorg. Chem.* **1991**, *30*, 2895–2899.

Published on Web 09/28/2010

charge transfer (LL′CT), and semiquinone and quinone species act as electron acceptors in metal-to-ligand charge-transfer (MLCT) states. Thus, the redox interconversions result in pronounced electrochromic behavior as well as switching between the number of electronic states present in a complex, which may be of interest for magnetic studies. Accordingly, metal dioxolene systems have been used in applications such as magnetic[5,11−18] and electrochromic materials,[2] as extended assemblies for electron and energy transfer incorporating both organic and coordination compounds, as components of modified electrodes, and as anchors to semiconductor surfaces[19−22] in applications related to solar energy conversion.[23−25]

Combining several dioxolene units into a single bridging ligand correspondingly increases the number of redox states accessible in a controlled fashion. We have shown how combining two catecholates "back to back" in the ligand 3,3′,4,4′-tetrahydroxybiphenyl (H_4biscat) results in dinuclear complexes having a reversible five-membered redox chain.[3,9] Combining three dioxolene units in a triangular array in the bridging ligand hexahydroxytriphenylene can result in trinuclear complexes with a reversible *seven*-membered redox chain in which all components have been spectroscopically characterized, and the complexes show exceptionally rich UV/vis/near-IR (NIR) electrochromic behavior.[26]

The research in this area has been focused mainly on catecholate complexes of d^6 metal centers,[27] such as ruthenium,[1−3,5−8,12,28−51] osmium,[3,39,40,48,51] chromium,[17] manganese,[25] and rhenium,[52,53] and on the properties of the electronic ground states of such compounds. In this paper, we report a detailed and extensive study on a series of mono- and dinuclear platinum(II) complexes based on dioxolene-type ligands coordinated to {Pt^{II}(diimine)} termini. While mononuclear complexes of the type {Pt^{II}(cat)(diimine)} (where "cat" denotes a general catecholate-type ligand) have been studied before, these studies have focused almost exclusively on the redox and spectroscopic properties of the electronic ground states of the complexes. Here we extend these studies, for the first time, to the electronic excited states using a range of ultrafast techniques [time-resolved infrared (TRIR) and UV/vis transient absorption (TA)], supported by density functional theory (DFT) calculations. We have also prepared a series of analogous dinuclear complexes based on the "back-to-back" bis-catecholate bridging ligand H_4biscat in which two [Pt^{II}(cat)(diimine)] units are connected via the "bis-catecholate" bridging ligand. These compounds too have been examined in both the ground [electrochemistry and UV/vis, IR, and electron paramagnetic resonance (EPR) spectroelectrochemistry] and excited states using picosecond TRIR and femtosecond UV/vis TA methods. The data obtained for the mononuclear complexes have been used to help interpret the results obtained for the dinuclear complexes. Overall, this paper includes the most detailed analysis yet reported of the ground- and excited-state electronic structures, and excited-state dynamics, of this class of complexes.

Results and Discussion

1. Synthesis and Characterization. Synthesis. The new platinum(II) complexes **1**−**6** were prepared as outlined in Schemes 1 and 2 and satisfactorily characterized by standard methods. The dinuclear complexes **1** and **2**, in which two Pt^{II} centers are bridged by the tetradentate bis-catechol ligand 3,3′,4,4′-tetrahydroxybiphenyl (H_4biscat)

(11) Patra, S.; Sarkar, B.; Mobin, S. M.; Kaim, W.; Lahiri, G. K. *Inorg. Chem.* **2003**, *42*, 6469–6473.
(12) Bhattacharya, S.; Pierpont, C. G. *Inorg. Chem.* **1994**, *33*, 6038–6042.
(13) Bag, N.; Pramanik, A.; Lahiri, G. K.; Chakravorty, A. *Inorg. Chem.* **1992**, *31*, 40–45.
(14) Fox, G. A.; Pierpont, C. G. *Inorg. Chem.* **1992**, *31*, 3718–3723.
(15) Shaikh, N.; Goswami, S.; Panja, A.; Wang, X. Y.; Gao, S.; Butcher, R. J.; Banerjee, P. *Inorg. Chem.* **2004**, *43*, 5908–5918.
(16) Kojima, T.; Nakanishi, T.; Harada, R.; Ohkubo, K.; Yamauchi, S.; Fukuzumi, S. *Chem.—Eur. J.* **2007**, *13*, 8714–8725.
(17) Wheeler, D. E.; McCusker, J. K. *Inorg. Chem.* **1998**, *37*, 2296–2307.
(18) Hartl, F.; Rosa, P.; Ricard, L.; Le Floch, P.; Zalis, S. *Coord. Chem. Rev.* **2007**, *251*, 557–576.
(19) Marczak, R.; Werner, F.; Gnichwitz, J. F.; Hirsch, A.; Guldi, D. M.; Peukert, W. *J. Phys. Chem. C* **2009**, *113*, 4669–4678.
(20) Gundlach, L.; Ernstorfer, R.; Willig, F. *Prog. Surf. Sci.* **2007**, *82*, 355–377.
(21) Gundlach, L.; Ernstorfer, R.; Willig, F. *Phys. Chem. Interface Nanomater. VI* **2007**, *6643*, I6430–I6430.
(22) Wang, Y. H.; Hang, K.; Anderson, N. A.; Lian, T. Q. *J. Phys. Chem. B* **2003**, *107*, 9434–9440.
(23) Boyer, J. L.; Rochford, J.; Tsai, M. K.; Muckerman, J. T.; Fujita, E. *Coord. Chem. Rev.* **2010**, *254*, 309–330.
(24) Das, D.; Mondal, T. K.; Mobin, S. M.; Lahiri, G. K. *Inorg. Chem.* **2009**, *48*, 9800–9810.
(25) Abuabara, S. G.; Cady, C. W.; Baxter, J. B.; Schmuttenmaer, C. A.; Crabtree, R. H.; Brudvig, G. W.; Batista, V. S. *J. Phys. Chem. C* **2007**, *111*, 11982–11990.
(26) Grange, C. S.; Meijer, A. J. H. M.; Ward, M. D. *Dalton Trans.* **2010**, 200–211.
(27) Spikes, G. H.; Bill, E.; Weyhermuller, T.; Wieghardt, K. *Angew. Chem., Int. Ed.* **2008**, *47*, 2973–2977.
(28) Auburn, P. R.; Dodsworth, E. S.; Haga, M.; Liu, W.; Nevin, W. A.; Lever, A. B. P. *Inorg. Chem.* **1991**, *30*, 3502–3512.
(29) Kar, P.; Verma, S.; Das, A.; Ghosh, H. N. *J. Phys. Chem. C* **2009**, *113*, 7970–7977.
(30) Chang, H. C.; Mochizuki, K.; Kitagawa, S. *J. Mol. Struct.* **2008**, *890*, 303–308.
(31) Mochizuki, K.; Kawamura, T.; Chang, H. C.; Kitagawa, S. *Inorg. Chem.* **2006**, *45*, 3990–3997.
(32) Monfette, S.; Fogg, D. E. *Organometallics* **2006**, *25*, 1940–1944.
(33) Okamura, R.; Wada, T.; Tanaka, K. *Bull. Chem. Soc. Jpn.* **2006**, *79*, 1535–1540.
(34) Takemoto, S.; Ogura, S.; Kamikawa, K.; Matsuzaka, H. *Inorg. Chim. Acta* **2006**, *359*, 912–916.
(35) Chang, H. C.; Mochizuki, K.; Kitagawa, S. *Inorg. Chem.* **2005**, *44*, 3799–3809.
(36) Fujihara, T.; Okamura, R.; Tanaka, K. *Chem. Lett.* **2005**, *34*, 1562–1563.
(37) Remenyi, C.; Kaupp, M. *J. Am. Chem. Soc.* **2005**, *127*, 11399–11413.
(38) Wada, T.; Tanaka, K. *Eur. J. Inorg. Chem.* **2005**, 3832–3839.
(39) Ye, S. F.; Sarkar, B.; Duboc, C.; Fiedler, J.; Kaim, W. *Inorg. Chem.* **2005**, *44*, 2843–2847.
(40) Fang, G. S.; Huang, J. S.; Zhu, N. Y.; Che, C. M. *Eur. J. Inorg. Chem.* **2004**, 1341–1348.
(41) Wada, T.; Fujihara, T.; Tomori, M.; Ooyama, D.; Tanaka, K. *Bull. Chem. Soc. Jpn.* **2004**, *77*, 741–749.
(42) Churchill, M. R.; Keil, K. M.; Gilmartin, B. P.; Schuster, J. J.; Keister, J. B.; Janik, T. S. *Inorg. Chem.* **2001**, *40*, 4361–4367.
(43) Churchill, M. R.; Keil, K. M.; Bright, F. V.; Pandey, S.; Baker, G. A.; Keister, J. B. *Inorg. Chem.* **2000**, *39*, 5807–5816.
(44) Rein, F. N.; Rocha, R. C.; Toma, H. E. *J. Electroanal. Chem.* **2000**, *494*, 21–29.
(45) Hill, P. L.; Lee, L. Y.; Younkin, T. R.; Orth, S. D.; McElwee-White, L. *Inorg. Chem.* **1997**, *36*, 5655–5657.
(46) Paw, W.; Keister, J. B.; Lake, C. H.; Churchill, M. R. *Organometallics* **1995**, *14*, 767–779.
(47) Bohle, D. S.; Carron, K. T.; Christensen, A. N.; Goodson, P. A.; Powell, A. K. *Organometallics* **1994**, *13*, 1355–1373.
(48) Bhattacharya, S.; Pierpont, C. G. *Inorg. Chem.* **1992**, *31*, 35–39.
(49) Carriedo, C.; Connelly, N. G. *J. Organomet. Chem.* **1991**, *403*, 359–363.
(50) Masui, H.; Lever, A. B. P.; Auburn, P. R. *Inorg. Chem.* **1991**, *30*, 2402–2410.
(51) Bhattacharya, S.; Boone, S. R.; Fox, G. A.; Pierpont, C. G. *J. Am. Chem. Soc.* **1990**, *112*, 1088–1096.
(52) Hartl, F.; Vlcek, A. *Inorg. Chem.* **1996**, *35*, 1257–1265.
(53) Hartl, F.; Vlcek, A. *Inorg. Chem.* **1992**, *31*, 2869–2876.

Scheme 1. Binuclear Catechol Complexes $\{Pt(R_2bpy)\}_2(biscat)$, Where R = ^{t}Bu or C(O)NEt$_2$

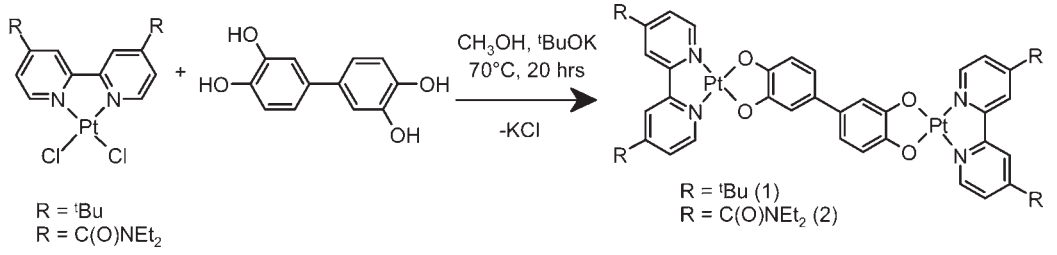

Scheme 2. Mononuclear Complexes Pt(R$_2$bpy)(Bu$_2$cat), Where R = H (**3**), ^{t}Bu (**4**), or C(O)NEt$_2$ (**5**), and Pt(dppe)(Bu$_2$cat) (**6**)[a]

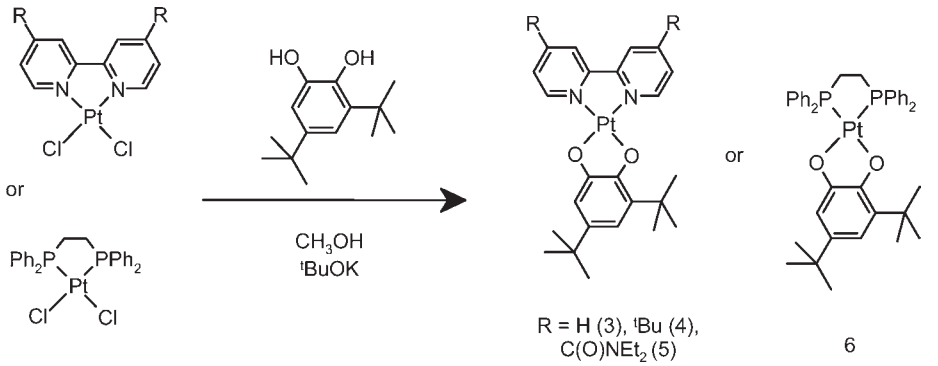

[a]dppe = diphenylphosphinoethane; Bu$_2$cat = 3,5-di-*tert*-butyl catecholate.

in its deprotonated form, were prepared by the reaction of 2 equiv of the appropriate Pt(diimine)Cl$_2$ with tetrahydroxybiphenyl in MeOH in the presence of 4 equiv of ^{t}BuOK. The diimine ligands used were 4,4′-di-*tert*-butyl-2,2′-bipyridine (^{t}Bu$_2$bpy) in **1** or 4,4′-(CONEt$_2$)$_2$-2,2′-bipyridine (bpyam) in **2**. The analogous mononuclear complexes Pt(diimine)(Bu$_2$cat) with unsubstituted 2,2′-bipyridine (**3**), ^{t}Bu$_2$bpy (**4**), and bpyam (**5**) were prepared by reaction of the appropriate Pt(diimine)Cl$_2$ precursor in MeOH with 3,5-di-*tert*-butylcatechol (H$_2$Bu$_2$cat) and 2 equiv of ^{t}BuOK. Attempts to prepare a dinuclear complex using unsubstituted 2,2′-bipyridine as the terminal diimine were unsuccessful because of the low solubility of the product, which precluded any purification. The mononuclear phosphine catecholate complex Pt(dppe)-(Bu$_2$cat) (**6**) was also prepared as a related catecholate-based platinum(II) complex that lacks the π-accepting diimine ligand. Catecholate/diimine complexes **1**−**5** were obtained as air-stable solids of deep-blue color; in contrast, the catecholate/diphosphine complex **6** was yellow.

The different diimine ligands were chosen to investigate the potential effect of their electron-accepting capability on the properties of the binuclear complexes because the ligand-based redox potentials will be sensitive to the presence of electron-donating (^{t}Bu) or accepting (amide) substituents. In addition, the presence of the amide substituents on the ligand bpyam in complexes **2** and **5** allows the carbonyl groups to be used as convenient spectroscopic handles for IR spectroscopy in both the ground and excited states of the complexes.

X-ray Crystallography. Mononuclear complexes **3** and **6** yielded X-ray quality crystals, from CH$_2$Cl$_2$/hexane or chloroform/hexane, respectively. ORTEP thermal ellipsoid plots, drawn at 80% probability, are shown in Figure 1; key metric data are summarized in the figure caption. The geometry around the central platinum atom in both cases is, predictably, close to square planar.

In **3**, the Pt−N bond lengths are in the range typical for platinum(II) diimine complexes; the dihedral angle between the N−Pt−N and O−Pt−O planes is 5.5°. There are four molecules in the unit cell of **3**, which are arranged in two parallel dimers, with the shortest Pt···Pt distance being 4.405 Å. The interplanar distance between two bipyridine ligands of the neighboring molecules of **3**, offset in the plane of the molecule with respect to one another, is 3.44 Å, implying a $\pi-\pi$ interaction between the diimine ligands. Complex **6** contains two crystallographically independent molecules in the asymmetric unit, with the dihedral angles between the P−Pt−P and O−Pt−O planes being 6.1 and 2.9°, respectively. There is no π stacking between ligands in **6**, and there are no short Pt···Pt contacts.

The O−Pt−O angle in both complexes is between 82 and 84°. This angle is considerably smaller than the S−Pt−S angle of 88.64(13)° observed in an analogous dithiolate compound, platinum (4,7-diphenyl-1,10-phenanthroline)-(3,5-di-*tert*-butylbenzene-1,2-dithiolate).[54] Examination of the structural parameters of the catecholate ligands (C−C and C−O distances) confirms in each case that these ligands are in the fully reduced dianionic catecholate oxidation state.[10,55,56]

2. Spectroscopic, Redox, and Spectroelectrochemical Properties in the Ground State. Electronic Absorption Spectroscopy. The absorption spectra of **1**−**5** in CH$_2$Cl$_2$

(54) Weinstein, J. A.; Tierney, M. T.; Davies, E. S.; Base, K.; Robeiro, A. A.; Grinstaff, M. W. *Inorg. Chem.* **2006**, *45*, 4544–4555.
(55) Sarkar, B.; Hübner, R.; Pattacini, R.; Hartenbach, I. *Dalton Trans.* **2009**, 4653–4655.
(56) Shavaleev, N. M.; Davies, E. S.; Adams, H.; Best, J.; Weinstein, J. A. *Inorg. Chem.* **2008**, *47*, 1532–1547.

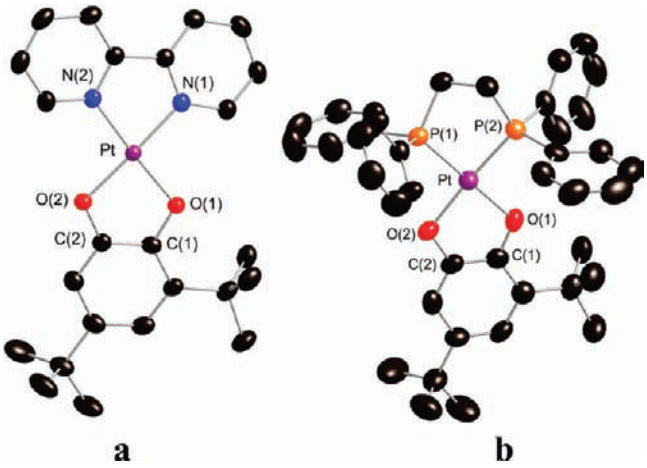

Figure 1. (a) X-ray structure of Pt(bpy)(Bu_2cat). 3.80% probability ellipsoids are shown. Selected bond distances (Å) and angles (deg): Pt−N(1), 1.9779(14); Pt−N(2), 1.9923(14); Pt−O(1), 1.9817(12); Pt−O(2), 1.9837(12); C(1)−O(1), 1.358(2); C(2)−O(2), 1.360(2); C(1)−C(2), 1.414(2); N(1)−Pt−N(2) 80.38(6); O(1)−Pt−O(2) 84.24(5). The dihedral angle between the N(1)−Pt−N(2) and O(1)−Pt−O(2) planes is 5.54°. (b) X-ray structure of Pt(dppe)(Bu_2cat). 6.80% probability ellipsoids are shown. Two types of coordination arrangements were detected. Molecule 1: Pt−P(1), 2.2164(11); Pt−P(2), 2.2200(12); Pt−O(1), 2.041(3); Pt−O(2), 2.056(3); C(1)−O(1), 1.340(5); C(2)−O(2), 1.370(5); C(1)−C(2), 1.412(6); P(1)−Pt−P(2), 86.23(5); O(1)−Pt−O(2) 82.41(11). The dihedral angle between the P(1)−Pt−P(2) and O(1)−Pt−O(2) planes is 2.90°. Molecule 2: Pt−P(1), 2.2026(12); Pt−P(2), 2.2215(12); Pt−O(1), 2.039(3); Pt−O(2), 2.040(3); C(1)−O(1), 1.367(5); C(2)−O(2), 1.368(5); C(1)−C(2), 1.410(6); P(1)−Pt−P(2), 85.93(5); O(1)−Pt−O(2) 83.31(11). The dihedral angle between the P(1)−Pt−P(2) and O(1)−Pt−O(2) planes is 6.09°.

are shown in Figure 2, and their key features are summarized in Table 1. All of the spectra have an absorption band in the wavelength range 390−440 nm, with an extinction coefficient in the range $(1-5)\times10^3$ L mol^{-1} cm^{-1}, which is similar to that observed in the dichloride precursor complexes [Pt(diimine)Cl_2].[57] This transition shifts to lower energies with an increase in the electron-accepting ability of the diimine ligand along the series ^{t}Bu_2bpy > bpy > bpyam and is attributed to a transition of predominantly Pt → diimine MLCT character. The absorption spectra of **1**−**5** also show an additional band centered at 580−690 nm, which is not present in the spectra of the Pt(diimine)Cl_2 precursors. The position of this absorption band also shifts to lower energy with an increase in the electron-accepting ability of the diimine ligand, indicating considerable involvement of the diimine-based orbitals in this electronic transition. This transition is assigned, on the basis of assignments in related palladium(II) and platinum(II) complexes, to a (predominantly) catecholate → diimine LL′CT, although this may also, on the basis of earlier studies, have some contribution from Pt d orbitals.[54] The extinction coefficient of this band is ca. 5×10^3 L mol^{-1} cm^{-1} for the mononuclear complexes **3**−**5**, similar to other platinum(II) diimine catecholate complexes.[54] However, the dinuclear complexes **1** and **2** show a much larger extinction coefficient for this transition, $(8-12)\times10^3$ L mol^{-1} cm^{-1}, consistent with the presence of two chromophoric centers. The absorption maxima of the binuclear complexes are only slightly shifted to lower energy compared to those of their mononuclear counterparts, indicating that the two catecholate

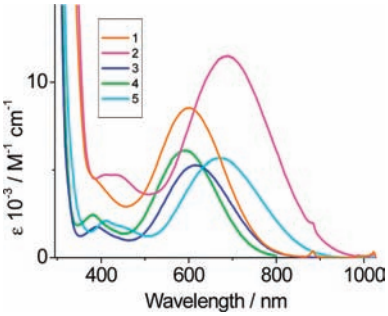

Figure 2. Electronic absorption spectra of complexes **1**−**5** in CH_2Cl_2.

units of **1** and **2** behave comparably to the isolated catecholate ligands of **3**−**5**, with little electronic communication between the two Pt(catecholate) centers, most likely because of a dihedral twist between them that is characteristic of biphenyl-type units.[58,59]

The lowest-energy absorption band in the electronic spectra of **1**−**5** exhibits negative solvatochromic behavior (Figure 3). The energy of this absorption band depends linearly on the solvent polarity parameter, with the gradient giving "solvatochromic shifts" of 5280 cm^{-1} for **3** and 6575 cm^{-1} for **2**, values typical for charge-transfer transitions.[60]

The nature of the highest occupied molecular orbital (HOMO) and lowest unoccupied molecular orbital (LUMO) involved in this transition will be discussed in further detail in the electrochemistry section below.

Cyclic Voltammetry (CV). CV data are presented in Figure 4 and are summarized in Table 1. Several electrochemically reversible redox processes are observed in the potential window between +0.5 and −2.0 V (vs Fc^+/Fc).

Reductions. All of the {Pt(diimine)(cat)} complexes show a single reversible one-electron (for complexes **3**−**5**) or two-electron (complexes **1** and **2**) redox process between −1.44 and −1.84 V. Because reduction of the corresponding Pt(diimine)Cl_2 complexes occurs in the same region, this process is attributed to reduction of the coordinated bipyridyl ligands. The Pt(dppe)(Bu_2cat) complex **6** does not show any reduction processes within the potential window examined, confirming the diimine-based nature of this process. This diimine-based reduction of the {Pt(diimine)(cat)} complexes **1**−**5** occurs at potentials some 80−150 mV more negative than those for their Pt(diimine)Cl_2 precursors, which is consistent with the more electron-donating nature of the catecholate ligand compared to the chloride. The facts that (i) the two diimine-based redox processes of the dinuclear complexes **1** and **2** occur sufficiently close together that they cannot be resolved by CV and (ii) this potential is very close (within 30 mV) to those from the mononuclear counterparts **4** and **5** both suggest that there is no electronic communication between the diimine ligands, which therefore behave as electrochemically isolated units, which is unsurprising given the separation between them.

Oxidations. All of the catecholate-containing complexes show their first oxidation process within the

(57) Weinstein, J. A.; Zheligovskaya, N. N.; Mel'nikov, M. Y.; Hartl, F. *J. Chem. Soc., Dalton Trans.* **1998**, 2459–2466.

(58) Eaton, V. J.; Steele, D. *J. Chem. Soc., Faraday Trans. 2* **1973**, 1601–1608.

(59) Brock, C. P.; Minton, R. P. *J. Am. Chem. Soc.* **1989**, *111*, 4586–4593.

(60) Cummings, S. D.; Eisenberg, R. *J. Am. Chem. Soc.* **1996**, *118*, 1949–1960.

Table 1. Electronic Absorption Spectra in CH_2Cl_2 and Redox Potentials of Compounds **1**−**6** and Corresponding Pt(diimine)Cl_2 Complexes Measured in CH_2Cl_2 Containing 0.2 M $[Bu_4N][PF_6]$, at Room Temperature

complex	λ_{max}/nm ($\varepsilon/10^{-3}$ M^{-1} cm^{-1})	$E_{1/2}$(red)/V ($\Delta E_{a,c}$/V) [a]	$E_{1/2}(ox_1)$/V	$E_{1/2}(ox_2)$/V
{Pt(^{t}Bu$_2$bpy)}$_2$(biscat) (**1**)	603 (8.5)	−1.84 (0.09)	−0.29 (0.08)	+0.05 (0.08)
{Pt(bpyam)}$_2$(biscat) (**2**)	691 (11.5), 430 (4.7)	−1.56 (0.08)	−0.29 (0.06)	−0.02 to +0.20
Pt(bpy)(Bu$_2$cat) (**3**)	618 (5.3), 390 (1.8)	−1.74 (0.08)	−0.14 (0.08)	
Pt(^{t}Bu$_2$bpy)(Bu$_2$cat) (**4**)[56]	577 (5.7), 377 (2.5)	−1.82 (0.08)	−0.18 (0.08)	
Pt(bpyam)(Bu$_2$cat) (**5**)	673 (5.7), 411 (2.1)	−1.59 (0.08)	−0.14 (0.07)	
Pt(dppe)(Bu$_2$cat) (**6**)	300 (8.27), 345 (sh, 3.93), 437 (0.48)		−0.25 (0.07)	+0.76 (0.12)
Pt(^{t}Bu$_2$bpy)Cl_2	388 (4.6)	−1.74 (0.09)		
Pt(bpyam)Cl_2	409 (5.0)	−1.44 (0.09)		

[a] The anodic−cathodic peak separations are given in parentheses. The values are reported versus Fc^+/Fc.

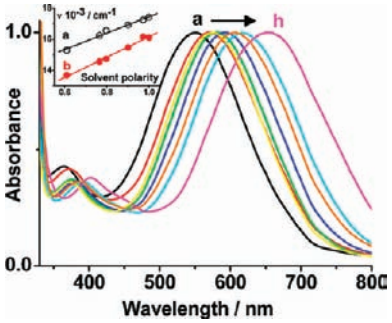

Figure 3. Normalized absorption spectra of complex **3** recorded in the following solvents: (a) methanol; (b) ethanol; (c) CH_3CN; (d) DMSO; (e) DMF; (f) acetone; (g) CH_2Cl_2; (h) $CHCl_3$. Inset: Linear dependence of the absorption maximum ν_{max} against the solvent polarity parameter[60] for (a) mononuclear complex **3** and (b) binuclear complex **2**.

range from −0.29 to −0.14 V vs Fc^+/Fc in CH_2Cl_2, a potential range typical for a catecholate^{2-}/semiquinone$^{\bullet-}$ (cat/sq)[61] interconversion of a coordinated dioxolene ligand. In the mononuclear complex **4**, this cat/sq redox process occurs at −0.18 V (vs Fc^+/Fc) in CH_2Cl_2.[56] The corresponding dinuclear complex **1** shows two reversible one-electron processes at −0.29 and +0.05 V assigned as two successive cat/sq redox processes associated with the bis-catecholate bridging ligand. These may be considered at one extreme as localized cat/sq couples, each associated with one aromatic ring, giving a mixed-valence state containing one catecholate and one semiquinone terminus. At the other extreme, each process may be considered as delocalized over the entire bridging ligand such that there is a fully delocalized intermediate cat/sq state in which the two dioxolene termini, and hence the two Pt^{II} centers, are equivalent to one another. The 340 mV separation between the two couples indicates that there is substantial electronic communication between the halves of the complex with a partly (or wholly) delocalized (cat/sq) mixed-valence state associated with the bridging ligand, which arises here because of the close proximity of the halves of the bridging ligand, which are directly connected. This behavior is in obvious contrast to the diimine-based redox processes, which are independent of one another because of the distance, and the lack of a direct connection, between them.

The mononuclear complex **5** shows a single one-electron-oxidation process at −0.14 V also due to this

(61) Throughout the text, "cat/sq" denotes a redox interconversion between catecholate^{2-} and semiquinone^{-} forms of a dioxolene ligand; "cat/sq" denotes the mixed-valence form of the biscat ligand after one-electron oxidation.

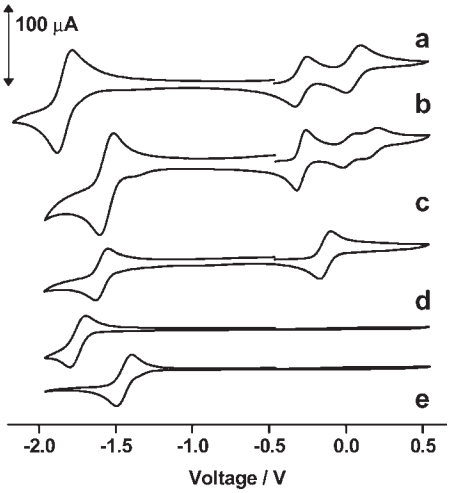

Figure 4. Cyclic voltammograms of ~1 mM solutions of (a) **1**, (b) **2**, (c) **5**, (d) Pt(^{t}Bu$_2$bpy)Cl_2, and (e) Pt((CONEt$_2$)$_2$bpy)Cl_2 in CH_2Cl_2 containing 0.2 M Bu_4NPF_6.

cat/sq couple. The dinuclear analogue **2** surprisingly shows a *single* reversible one-electron cat/sq process at −0.29 V. Notably, the second redox process appears as two consecutive half-intensity waves between −0.02 and +0.20 V, each formally amounting to a "half-electron" transfer. This unusual behavior is tentatively attributed to dimerization between molecules on the electrode surface once half of the molecules have undergone the second redox process to generate the bridging ligand in the sq/sq state. Such dimerization, involving a sq/cat and a sq/sq species in each dimer, would cause an increase in the potential necessary to oxidize the remaining half of the sq/cat molecules to the sq/sq state, as illustrated in Scheme 3. A similar redox behavior interpreted in terms of dimerization has recently been observed for Pt(^{t}Bu$_2$bpy)(cat-R), where R = 1,8-naphthalenemonoimide and derivatives or 1,4,5,8-naphthalenediimide, and has been analyzed by us in detail.[56] Additional support for the dimerization hypothesis comes from the fact that the much more soluble dinuclear complex **1** does not show this unusual behavior (see above).

UV/Vis/NIR Spectroelectrochemistry. To obtain further insight into the nature and localization of the redox processes and the localization of the frontier orbitals in **1**−**5**, UV/vis/NIR spectroelectrochemical experiments were performed in CH_2Cl_2 in the range 250−3000 nm. It was noted that for **5** precipitation of the oxidized complex occurred during the course of the electrochemical experiments, possibly because of the presence of the

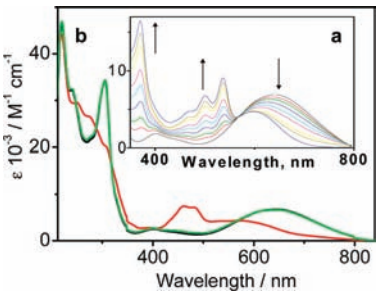

Figure 5. (a) Spectral changes accompanying the first reduction process of **5** in CH_2Cl_2 with 0.2 M Bu_4NPF_6 at 253 K. Note the thermochromic shift of the absorption maximum to 640 nm at 253 K if compared to that at room temperature. The extinction coefficients (10^3 L mol^{-1} cm^{-1}) of the principal bands of $\mathbf{5}^{\bullet-}$ are as follows: 370 nm (16.5), 468 nm (sh, 4.74), 500 nm (6.77), 536 nm (9.06), 595 nm (4.71). (b) Spectral changes accompanying the first oxidation process of **5** in CH_2Cl_2 with 0.2 M Bu_4NPF_6 at 253 K. Color code: black, initial spectrum of a neutral species; red, spectrum of $\mathbf{5}^{\bullet+}$; green, spectrum after the rereduction of $\mathbf{5}^{\bullet+}$ to **5**.

Scheme 3. Proposed Processes Accompanying Oxidation of Binuclear Complex **2** [M = Pt(bpyam)] in CH_2Cl_2

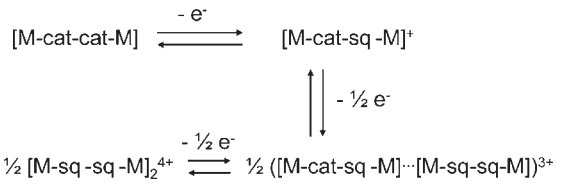

supporting electrolyte; hence, chemical oxidation in CH_2Cl_2 with $[FeCp_2]PF_6$ or Me_4NBr_3 was also used. Where both methods were employed, the results obtained by electrochemical and chemical oxidations are identical.

Reduction. The first (diimine-based) reduction process in complexes **1**−**5** is accompanied by a bleach of the cat → diimine LL′CT absorption band at ca. 600 nm, and the appearance of new narrow bands at 370, 465, 500, and 535 nm. These are characteristic of a coordinated bipyridyl radical anion,[62] and hence the results are consistent with the LUMO being localized predominantly on the bipyridyl ligand in all cases, as described above. Figure 5a shows a representative example of the spectroscopic data obtained during the electrochemical reduction of complex **5** to $[\mathbf{5}]^{\bullet-}$.

Oxidation. Oxidation of the mononuclear catecholate-containing complexes is accompanied by a decrease in the intensity of the LL′CT absorption band (lowest-energy feature) and the development of new higher-energy peaks at 460, 480, and 575 nm. Representative spectra obtained for $[\mathbf{5}]^{\bullet+}$ generated electrochemically are shown in Figure 5b. The virtually identical results obtained by the chemical oxidation of **4** by $[FeCp_2]PF_6$ are shown in the Supporting Information. The new spectral features are identical with those reported previously for the catecholate-based oxidation of various {Pt(diimine)(cat)} complexes[54,56] and are characteristic of a coordinated semiquinone radical. Hence, the spectroelectrochemical results confirm that the HOMO of the mononuclear complexes **3** and **5** is predominantly catecholate-based.

The first one-electron oxidation of the dinuclear complex **1** in CH_2Cl_2 shows new peaks growing in at 435, 475, and 605 nm, concomitant with bleaching of the MLCT/LL′CT absorption band (Figure 6). These features are very similar to those seen in the radical cation of the mononuclear complexes (Figure 5), indicative of a coordinated semiquinone fragment. However, for $[\mathbf{1}]^{\bullet+}$, a new strong absorption band in the NIR region is observed at 1425 nm (ε = 19 100 M^{-1} cm^{-1}), with a shoulder at 1150 nm, which has no counterpart in the spectra of the oxidized mononuclear complexes. The most likely assignment of this is an intraligand catecholate → semiquinone transition associated with the [cat/sq] form of the bridging ligand. In a localized description of the mixed-valence state, this would be a transition from the HOMO of the catecholate fragment (on one aromatic ring) to the singly occupied molecular orbital (SOMO) of the semiquinoidal fragment (on the other), a ligand-based intervalence charge-transfer (IVCT) transition. In a delocalized description, this would be a $\pi-\pi^*$ transition of the entire bridging ligand system with no vectorial electron transfer.

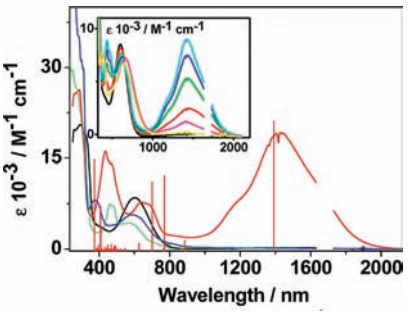

Figure 6. Absorption spectra of **1** in different redox states: black, neutral; red, one-electron-oxidized species $\mathbf{1}^{\bullet+}$ obtained by the chemical oxidation with Fc^+; blue, two-electron-oxidized species $\mathbf{1}^{2+}$ obtained by the chemical oxidation with Me_4NBr_3 in CH_2Cl_2 at room temperature. The spectrum of the electrochemically generated radical cation of **5** is shown for comparison (green line). Extinction coefficients (10^3 L mol^{-1} cm^{-1}) of the principal bands are as follows. $\mathbf{5}^{\bullet+}$: 460 nm (7.4), 483 nm (7.1), 575 nm (4.3). $\mathbf{1}^{\bullet+}$: 435 nm (16.1), 465 nm (14.2), 640 nm (7.8), 685 nm (7.4), 1160 nm (7.2), 1425 nm (19.1). $\mathbf{1}^{2+}$, 375 nm (7.7), 586 nm (7.1). Red sticks represent the calculated spectrum of the radical cation $[\{Pt(bpy)\}_2(biscat)]^{\bullet+}$. Inset: Spectral changes accompanying the chemical oxidation of $\{Pt(^tBu_2bpy)\}_2(biscat)$ in CH_2Cl_2 with Me_4NBr_3.

Such $\pi-\pi^*$ transitions of "class 3" mixed-valence compounds are characteristically narrow, and the full-width at half-maximum (fwhm) of the absorption band corresponding to this transition is consistent with this assignment. Equation 1, which holds for class 2 (localized) mixed-valence species, predicts that the value of $\Delta\nu_{1/2}$ for a class 2 IVCT transition at 1425 nm should be ca. 4000 cm^{-1}.[63,64] In fact, the observed value of $\Delta\nu_{1/2}$ is clearly much less than this: the width at half-height of this low-energy absorption manifold is ca. 2000 cm^{-1}, and because there is clearly a shoulder on the high-energy side, this will be an overestimate of the value of $\Delta\nu_{1/2}$. Thus, the small fwhm of the low-energy absorption is indicative of class 3 (fully delocalized) behavior for the mixed-valence cat/sq state. This is also consistent with the redox splitting of 340 mV between successive cat/sq couples, which implies substantial delocalization in the ligand-centered mixed-valence state; this, in turn, might be expected to require the cat/sq bridging ligand to be planar.

(62) Krejčik, M.; Vlček, A. A. *J. Electroanal. Chem. Interfacial Electrochem.* **1991**, *331*, 243–257.

(63) Creutz, C. *Prog. Inorg. Chem.* **1983**, *30*, 1–73.

(64) Richardson, D. E.; Taube, H. *Coord. Chem. Rev.* **1984**, *60*, 107–129.

We return to this point later.

$$\Delta\nu_{1/2} = (2310E)^{1/2} \quad (1)$$

The second oxidation process leads to the disappearance of this NIR absorption band, confirming its intraligand nature, and the involvement of both semiquinone and catecholate components. This oxidation process generates the bridging ligand in the [sq/sq] state, which, as described earlier, is expected to be planar with substantial C=C double-bond character between the rings.[9] This redox process is also accompanied by the appearance of new bands of modest intensity at ca. 600 and 375 nm.

The two bridging ligand-centered processes are fully chemically reversible, as confirmed by a full restoration of the original spectral profile upon rereduction of the system and identical CV profiles for the neutral and one-electron-oxidized species. Chemical oxidation of **1** by titration with Me_4NBr_3 also allowed us to generate both mono- and dioxidized species $[\mathbf{1}]^{\bullet+}$ and $[\mathbf{1}]^{2+}$ by chemical means, and evolution of the electronic spectra was identical with that observed in the spectroelectrochemical experiment.

EPR Spectra of $[\mathbf{1}]^{\bullet+}$ and $[\mathbf{1}]^{\bullet-}$. EPR spectra of $[\mathbf{1}]^{\bullet+}$ and $[\mathbf{1}]^{\bullet-}$ were recorded to examine further the extent of metal contribution to the frontier orbitals and the possibility of charge delocalization. The experiments were performed in CH_2Cl_2 for solubility reasons. In the reduction experiments, samples for study were removed from the electrolysis cell after the passing of one electron per molecule (i.e., one electron per *two* Pt centers) and the frozen-solution X-band EPR spectrum was recorded at 77 K. The spectra obtained were generally consistent with the spectral profile obtained from reduction of analogous mononuclear [Pt(4,4′-R_2-bpy)(cat)] complexes. The spectrum was satisfactorily simulated using three g components ($g_{xx} = 1.999$, $g_{yy} = 2.034$, and $g_{zz} = 1.923$). Platinum hyperfine coupling was distinguished on the g_{xx} and g_{yy} components of the signal with values obtained from the simulation of $A_{xx} = 78.4 \times 10^{-4}$ cm^{-1} and $A_{yy} = 60.8 \times 10^{-4}$ cm^{-1}. For g_{zz} (1.923), which appeared as a broad feature, well-resolved coupling was not observed, but the shape was better reproduced by the inclusion of some metal hyperfine contribution ($A_{zz} = 39.5 \times 10^{-4}$ cm^{-1}; Figure 7).

The presence of hyperfine coupling to only one Pt center confirms that the diimine-based radical anion is localized at one end of the complex, which is consistent with the electrochemical data (two diimine-based reductions coincide) and is to be expected given the distance between the two diimine termini. Attempts to generate $[\mathbf{1}]^{2-}$ by further reduction were unsuccessful because of slow decomposition of the product on the slow time scale of bulk electrolysis.

The electrochemical oxidation of a 1 mM solution of **1** in CH_2Cl_2 containing either $[Bu_4N][BF_4]$ (0.4 M) or $[Bu_4N][PF_6]$ (0.1 M) was performed at the applied potential 0.44 V vs SCE, sufficient to complete the first oxidation only and generate the cat/sq state of the bridging ligand. This process resulted in the formation of a green solution and the precipitation of a dark-green solid. EPR spectroscopy of the solution at ambient temperature gave a weak signal at $g_{iso} = 2.0005$ with no obvious metal hyperfine coupling. Upon cooling the solution to 77 K, no signal was observed, suggesting aggregation/dimerization of the cations upon cooling (cf. the behavior of **2** in CV experiments, see above).

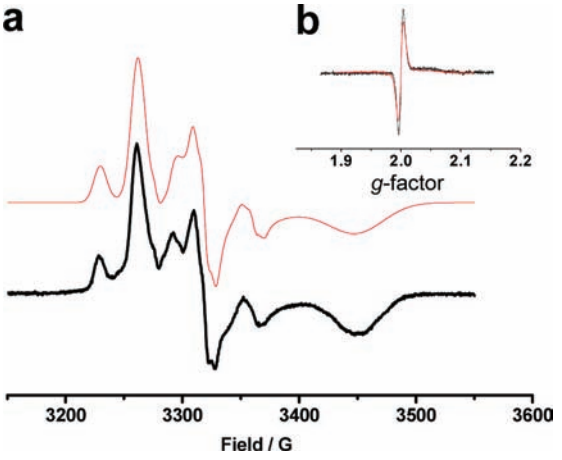

Figure 7. (a) EPR spectrum of the monoanion of {Pt(^{t}Bu$_2$bpy)}$_2$(biscat), which was generated electrochemically from ca. 1 mM solution in CH_2Cl_2 in the presence of 0.4 M Bu_4NPF_6 at room temperature (thick black line). The spectrum was recorded at 77 K. Thin red line: simulation with the parameters specified in the text and Gaussian line shapes with line widths of 13, 12, and 30 G in x, y, and z, respectively. (b) EPR spectra of the binuclear complex {Pt(^{t}Bu$_2$bpy)}$_2$(biscat) obtained after one-electron oxidation by electrochemical (black) and chemical (red) routes.

This result, along with the results of the CV studies, indicates that the oxidation and, therefore, the HOMO of the neutral species are localized on the bis-catecholate ligand but with no detectable contribution from the Pt center. This behavior is different from that observed for several mononuclear platinum(II) diimine catecholate compounds for which the EPR spectrum of a monocation shows that the SOMO contains a contribution of several percent from the Pt center.[54]

IR Spectroscopy and IR Spectroelectrochemistry. The IR spectra of all of the complexes studied are dominated by the vibrations related to the catecholate moiety, as is evident from the similarity between the spectra of the dppe complex **6** and the diimine complexes (Figure 8), which have only the catecholate ligand in common; the assignments given below are supported by DFT calculations. The mononuclear catecholate complexes **3**−**6** show a characteristic pattern of two strong bands, due to ν(CO) stretches coupled to the catecholate ring vibration, at 1240 and 1280 cm^{-1}. Two weaker bands are also present at 1201 and 1320 cm^{-1} [skeletal catecholate ring vibrations/ν(CO)]. The positions of these bands are virtually unaffected by the change of the diimine/dppe coligand. Another characteristic pair of bands, at 1420 and 1440 cm^{-1}, is due to ν(CO)/ν(CC) (cat), with weaker bands at 1470 and 1481 cm^{-1} having ν(CC) (cat)/δ(CH) character. The dinuclear biscatecholate complexes **1** and **2** show strong bands at 1252 and 1474 cm^{-1}, which are assigned to the skeletal modes of the entire biscat unit involving ring stretches, ν(CO), δ(CH), and ν(CC) of the bridging −CC− bond linking the two catecholate units. Weak bands due to catecholate units are also present at ∼1600 and 1570 cm^{-1}.

In complexes **1**−**5**, weak bands attributed to bipyridine vibrations are present in the 1520−1580 cm^{-1} range. The band due to the bipyridine ring stretching/CN vibration

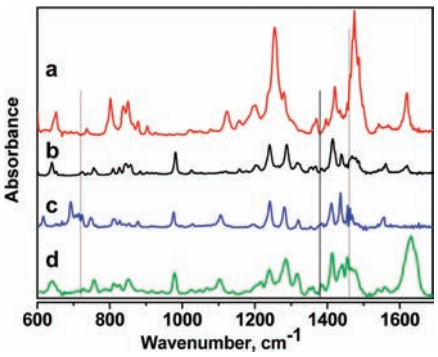

Figure 8. IR spectra of **1** (a), **4** (b), **6** (c), and **5** (d) in Nujol mull. Black lines correspond to the positions of the main Nujol bands.

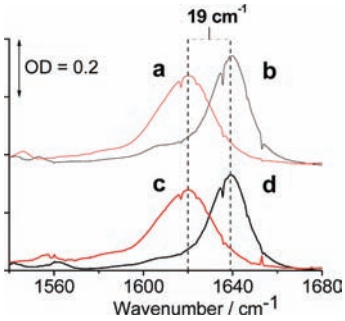

Figure 9. Changes in the IR spectra accompanying one-electron reduction of complexes **2** and **5** in CH_2Cl_2 containing 0.2 M Bu_4NPF_6: (a) $[\mathbf{2}]^{\bullet-}$; (b) neutral **2**; (c) $[\mathbf{5}]^{\bullet-}$; (d) neutral **5**.

appears at 1620 cm^{-1} in the diimine complexes, but in the spectra of **2** and **5**, it is obscured by ν(CO) of the amide group at 1639 cm^{-1}.

Upon one-electron reduction, the behavior of the bpyam-containing complexes [Pt(bpyam)Cl_2], mononuclear **5**, and binuclear **2** were all very similar, with a decrease in ν(C=O) of the amide group by 19 cm^{-1} (Figure 9). Such a decrease in the energy of ν(C=O) is due to population of the LUMO, which is a diimine-centered π^*-antibonding orbital, resulting in a weaker C=O bond and a shift to lower energy.

Oxidation of complexes **2** and **5** resulted in only a very small shift of ν(C=O) (<3 cm^{-1}) consistent with the HOMO being catecholate-based and therefore hardly affecting the terminal diimine ligands. Instead, oxidation of the complexes results in noteworthy changes occurring in the catechol-dominated mid-IR region from 1200 to 1600 cm^{-1}, as shown in the example of oxidation of **4** (Figure 10) performed in CD_3CN in the presence of KPF_6 as the supporting electrolyte. Upon one-electron oxidation of **4**, the bands attributed to the coordinated catecholate ligand at 1243, 1288, and 1319 cm^{-1} diminish in intensity, and the intensity of the 1470 cm^{-1} and 1484 cm^{-1} bands also decrease, which confirms transformation of the catecholate form of the ligand in accordance with the HOMO being catecholate-based.

DFT calculations predict two CO/CC stretches for the neutral form of **1** and **4**, at ca. 1600 and 1570 cm^{-1} after application of a typical scaling factor of 0.98. Importantly, vibrational displacement analysis points out that there is no direct equivalent of the 1570 cm^{-1} band in the IR spectrum of the cations $[\mathbf{1}]^{\bullet+}$ and $[\mathbf{4}]^{\bullet+}$. According to calculations, the 1600 cm^{-1} ν(CO/CC) band is predicted to shift to lower energies upon oxidation of the catecholate ligand to the semiquinoidal form; this accounts for the band at 1575 cm^{-1} detected in $[\mathbf{4}]^{\bullet+}$ and also accounts for the vibration detected in this range in the triplet excited state (see the TRIR section below).

The formation of this new band, in the range 1565−1585 cm^{-1}, was observed for the radical cations of all complexes studied. In all cases, spectra were assigned, by comparison with the IR spectra of the catecholate ligands and with the aid of DFT calculations, to intraring stretching vibrations of the semiquinoidal form of the catecholate ligand. This band is significant for the purpose of the present study because it will be used as a marker of the catechol → semiquinone transformation in the TRIR studies described below.

3. Excited-State Structure and Dynamics Studied by Ultrafast Transient Spectroscopy. Picosecond TRIR Studies. TRIR[65−84] was used to probe the nature and dynamics of the excited state of the binuclear complexes **1** and **2**, their mononuclear counterparts **4** and **5**, and one of the corresponding chloride precursors [Pt(bpyam)Cl_2] in the spectral range from 1490 to 1670 cm^{-1}.

Pt(bpyam)Cl_2. Excitation at 400 nm with a 150 fs laser pulse populates the Pt^{II} → bpyam ^{1}MLCT excited

(65) Weinstein, J. A.; Blake, A. J.; Davies, E. S.; Davis, A. L.; George, M. W.; Grills, D. C.; Lileev, I. V.; Maksimov, A. M.; Matousek, P.; Mel'nikov, M. Y.; Parker, A. W.; Platonov, V. E.; Towrie, M.; Wilson, C.; Zheligovskaya, N. N. *Inorg. Chem.* **2003**, *42*, 7077–7085.
(66) Kuimova, M. K.; Mel'nikov, M. Y.; Weinstein, J. A.; George, M. W. *J. Chem. Soc., Dalton Trans.* **2002**, 2857–2861.
(67) Weinstein, J. A.; Grills, D. C.; Towrie, M.; Matousek, P.; Parker, A. W.; George, M. W. *Chem. Commun.* **2002**, 382–383.
(68) Glik, E. A.; Kinayyigit, S.; Ronayne, K. L.; Towrie, M.; Sazanovich, I. V.; Weinstein, J. A.; Castellano, F. N. *Inorg. Chem.* **2008**, *47*, 6974–6983.
(69) Whittle, C. E.; Weinstein, J. A.; George, M. W.; Schanze, K. S. *Inorg. Chem.* **2001**, *40*, 4053–4062.
(70) Kovelenov, Y. A.; Blake, A. J.; George, M. W.; Matousek, P.; Mel'nikov, M. Y.; Parker, A. W.; Sun, X. Z.; Towrie, M.; Weinstein, J. A. *Dalton Trans.* **2005**, 2092–2097.
(71) Towrie, M.; Grills, D. C.; Dyer, J.; Weinstein, J. A.; Matousek, P.; Barton, R.; Bailey, P. D.; Subramaniam, N.; Kwok, W. M.; Ma, C. S.; Phillips, D.; Parker, A. W.; George, M. W. *Appl. Spectrosc.* **2003**, *57*, 367–380.
(72) Adams, C. J.; Fey, N.; Harrison, Z. A.; Sazanovich, I. V.; Towrie, M.; Weinstein, J. A. *Inorg. Chem.* **2008**, *47*, 8242–8257.
(73) Butler, J. M.; George, M. W.; Schoonover, J. R.; Dattelbaum, D. M.; Meyer, T. J. *Coord. Chem. Rev.* **2007**, *251*, 492–514.
(74) Chen, P. Y.; Palmer, R. A. *Appl. Spectrosc.* **1997**, *51*, 580–583.
(75) Easun, T. L.; Alsindi, W. Z.; Deppermann, N.; Towrie, M.; Ronayne, K. L.; Sun, X. Z.; Ward, M. D.; George, M. W. *Inorg. Chem.* **2009**, *48*, 8759–8770.
(76) Gabrielsson, A.; Hartl, F.; Zhang, H.; Smith, J. R. L.; Towrie, M.; Vlcek, A.; Perutz, R. N. *J. Am. Chem. Soc.* **2006**, *128*, 4253–4266.
(77) Rubtsov, I. V.; Redmore, N. P.; Hochstrasser, R. M.; Therien, M. J. *J. Am. Chem. Soc.* **2004**, *126*, 2684–2685.
(78) Sazanovich, I. V.; Alamiry, M. A. H.; Best, J.; Bennett, R. D.; Bouganov, O. V.; Davies, E. S.; Grivin, V. P.; Meijer, A.; Plyusnin, V. F.; Ronayne, K. L.; Shelton, A. H.; Tikhomirov, S. A.; Towrie, M.; Weinstein, J. A. *Inorg. Chem.* **2008**, *47*, 10432–10445.
(79) Schoonover, J. R.; Shreve, A. P.; Dyer, R. B.; Cleary, R. L.; Ward, M. D.; Bignozzi, C. A. *Inorg. Chem.* **1998**, *37*, 2598–2601.
(80) Schoonover, J. R.; Strouse, G. F. *Chem. Rev.* **1998**, *98*, 1335–1355.
(81) Turner, J. J. *Coord. Chem. Rev.* **2002**, *230*, 213–224.
(82) Weinstein, J. A.; van Slageren, J.; Stufkens, D. J.; Zalis, S.; George, M. W. *J. Chem. Soc., Dalton Trans.* **2001**, 2587–2592.
(83) Ball, G. E.; Brookes, C. M.; Cowan, A. J.; Darwish, T. A.; George, M. W.; Kawanami, H. K.; Portius, P.; Rourke, J. P. *Proc. Natl. Acad. Sci. U.S.A.* **2007**, *104*, 6927–6932.
(84) Kuimova, M. K.; Alsindi, W. Z.; Dyer, J.; Grills, D. C.; Jina, O. S.; Matousek, P.; Parker, A. W.; Portius, P.; Sun, X. Z.; Towrie, M.; Wilson, C.; Yang, J. X.; George, M. W. *Dalton Trans.* **2003**, 3996–4006.

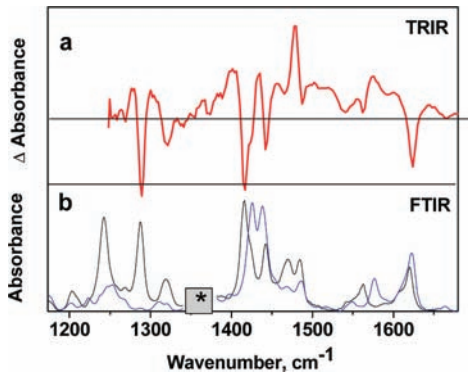

Figure 10. (a) TRIR spectrum of **4**, recorded in CD_3CN at a 2 ps delay after a 400 nm, 40 fs laser pulse. (b) Changes in the IR spectra accompanying one-electron oxidation of complex **4**, Pt(^{t}Bu$_2$bpy)(Bu$_2$cat), in CD_3CN in the presence of KPF_6. Color code: black, neutral species; blue, oxidized species. The asterisk indicates the area of insufficient background subtraction.

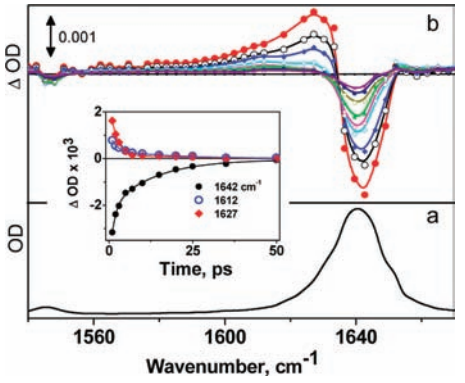

Figure 11. (a) Ground-state FTIR spectrum and (b) a series of TRIR spectra of Pt(bpyam)Cl_2 in CH_2Cl_2, recorded at 1, 2, 3, 7, 15, 20, and 25 ps time delays after initial excitation with a 400 nm, ~150 fs laser pulse. The inset shows the kinetic traces recorded at 1642 cm^{-1} (parent bleach recovery) and a transient decay at 1612 and 1627 cm^{-1}. Solid lines on the kinetic traces correspond to biexponential fits to the data with 1.9 ± 0.4 and 17 ± 4 ps lifetimes in all cases.

state directly. The spectrum after 1 ps shows a bleach of the parent ν(CO) of the amide group at 1640 cm^{-1} and formation of a transient band at 1624 cm^{-1} as resolved by a multi-Lorentzian fit to the data (Figure 11). The weak band at 1545 cm^{-1} was also bleached upon excitation, being replaced by a broad transient manifold over the range 1515−1540 cm^{-1}, whose low intensity precluded following its dynamics. The shift of the main ν(CO) to lower energy by 16 cm^{-1} upon formation of the excited state is consistent with the MLCT assignment of this excited state,[67,68] in which population of the bpyam π^* orbitals increases the electron density in the antibonding orbital of the CO group. The position of ν(CO) in the excited state corresponds closely to ν(CO) in the radical anion [Pt(bpyam)Cl_2]$^{\bullet-}$ obtained spectroelectrochemically, further supporting the MLCT assignment. The excited state recorded with TRIR is likely to be a vibrationally hot ^{3}MLCT state due to ultrafast intersystem crossing from the initially populated ^{1}MLCT state, which for this type of complex is anticipated at the time scale of several tens of femtoseconds.[85−87]

Several components contribute to the excited-state dynamics (Figure 11, inset). The main intense 1624 cm^{-1} ν(CO) transient band decays with a lifetime of 1.9 ps. This lifetime is attributed to back electron transfer in the ^{3}MLCT excited state to create a vibrationally excited ground state that relaxes through intramolecular vibrational relaxation and cooling. The transient IR spectrum of Pt(bpyam)Cl_2 does not decay completely on this time scale but generates a residual longer-lived weak and broad transient band in the range 1611−1625 cm^{-1}, which decays completely with a lifetime of 17 ± 4 ps. Recovery of the parent spectrum occurs in a biexponential fashion with lifetimes of 1.9 ± 0.4 and 17 ps, exactly matching the two decays of the transient bands from the excited state. A similar observation was made previously while investigating the excited-state dynamics of Pt(4,4′-{CO_2-nonyl}$_2$-2,2′-bpy)Cl_2 by a combination of TRIR and TA spectroscopies.[68] Two tentative assignments of the longer lifetime were proposed that cannot be distinguished on the basis of our data. One suggestion was to attribute the longer lifetime to the d−d excited state, through which decay of CT excited states is postulated to occur in this type of complex. Another possibility is that the longer (17 ps) lifetime is due to decay of a vibrationally hot electronic ground state. Such a state is likely to be formed in the course of back electron transfer in the ^{3}MLCT state because approximately 2 eV of energy will be dissipated in the course of 2 ps, and we therefore favor the latter interpretation.

Catecholate Complexes. Excitation of a solution of dinuclear **1** or **2** or their mononuclear analogues **4** and **5** in dichloromethane at 400 nm, using a ~150 fs laser pulse (**2** and **5**) or a ~40 fs pulse (**1** and **4**), leads to instant depletion of the ground-state IR bands and formation of transient bands shifted to lower energies (Figure 12).

In amide-containing **2** and **5**, the 1639 cm^{-1} ν(CO) band of the bpyam ligand shifts to 1625 cm^{-1} upon promotion to the excited state, confirming the CT-to-diimine nature of the lowest electronic transition that populates a bpyam ligand-based π^* orbital, which is antibonding with respect to the carbonyl group of the amide ligand. This negative shift observed for ν(CO) is very similar to that observed by IR spectroelectrochemistry upon formation of the corresponding radical anions [**2**]$^{\bullet-}$ and [**5**]$^{\bullet-}$ (Figures 9 and 12). The fact that the change in energy of ν(CO) in the excited state is virtually identical for **2** and **5** and also with that of the electrochemically generated radical anion strongly indicates that the (bpyam)$^{\bullet-}$ units formed in every case are in essentially the same chemical environment and that in the excited state of the dinuclear complex the reduced (bpyam)$^{\bullet-}$ unit is valence-localized, as shown by the electrochemical and spectroelectrochemical results earlier. (In principle, the same result could be observed if both Pt^{II} centers in **2** were simultaneously promoted to the excited state upon excitation, with both bpyam ligands transiently reduced to (bpyam)$^{\bullet-}$; this

(85) Cannizzo, A.; van Mourik, F.; Gawelda, W.; Zgrablic, G.; Bressler, C.; Chergui, M. *Angew. Chem., Int. Ed.* **2006**, *45*, 3174–3176.

(86) Damrauer, N. H.; McCusker, J. K. *J. Phys. Chem. A* **1999**, *103*, 8440–8446.

(87) Cannizzo, A.; Blanco-Rodriguez, A. M.; El Nahhas, A.; Sebera, J.; Zalis, S.; Vlcek, A.; Chergui, M. *J. Am. Chem. Soc.* **2008**, *130*, 8967–8974.

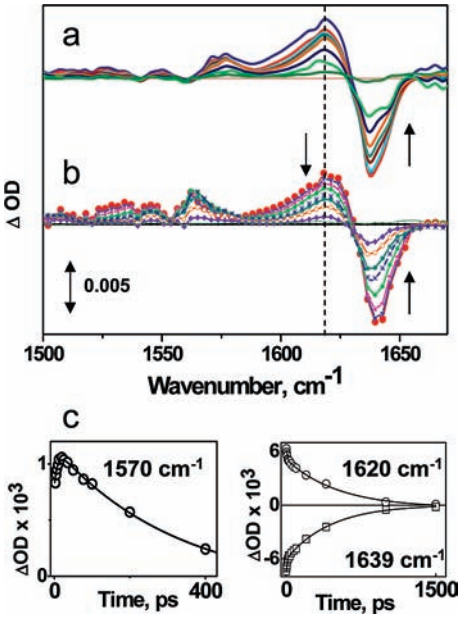

Figure 12. TRIR data obtained in CH_2Cl_2 following excitation with a 400 nm, ~150 fs laser pulse: (a) a series of TRIR spectra for the mononuclear complex **5**, recorded at −50, 1, 2, 3, 7, 35, 100, 200, 400, and 1000 ps time delays after the laser pulse; (b) a series of TRIR spectra for the binuclear complex **2**, recorded at 2, 3, 7, 15, 35, 75, 200, and 400 ps time delays after the laser pulse; (c) initial parts of the kinetic trace recorded at 1570 cm^{-1}, which demonstrate the presence of a grow-in component for **2**, the parent bleach recovery of ν(CO) at 1639 cm^{-1} for **5**, and the decay of the corresponding transient band at 1620 cm^{-1} for **5**.

scenario is, however, extremely unlikely given the very low photon densities used. The data are therefore interpreted assuming that only one Pt^{II} center per molecule of binuclear complex is excited at any one time.)

In the case of **1** and **4**, which have no amide substituents, the ν(CN) band of the coordinated bipyridyl ligand at 1624 cm^{-1} was not obscured by the intense ν(CO) as in the bpyam complexes. Upon excitation, this ν(CN) band is bleached and shifted to 1600 cm^{-1}, in accordance with population of the π^*-antibonding orbital of the bpy ligand in the LL′CT excited state. For all of the catecholate complexes studied, formation of a 1564−1575 cm^{-1} transient band in the excited state was also observed, attributed to a combined ν(CO/CC) vibration due to the presence of a semiquinoidal unit (cf. the ground-state IR spectroelectrochemical data). The TRIR spectra of **4** were also recorded in CD_3CN in the region 1200−1700 cm^{-1} in order to access the modes associated with ν(CO) of the catecholate ligand (Figure 10). The bleach of the band of the ground state at 1289 cm^{-1} attributed to ν(CO) of the coordinated catecholate ligand is indeed observed.

Overall, the IR spectra of the excited states of **1**, **2**, **4**, and **5** contain both the semiquinone-based bands associated with the radical cation (as obtained from IR spectroelectrochemical studies; Figure 10) and those of the coordinated diimine radical anion, confirming the catecholate-to-diimine LL′CT nature of the lowest excited state.

A global fit of the kinetic data resolved three lifetime components for the excited-state dynamics for all complexes studied. An ultrafast component (<1 ps) is present that is tentatively attributed to vibrational relaxation of the initially formed MLCT/LL′CT state, perhaps synchronous with completion of the charge separation. This state is expected to be formed vibrationally hot following 400 nm ultrafast excitation.

All transient bands, apart from those at 1564−1575 cm^{-1}, exhibit further two-exponential decay with lifetimes of several picoseconds and several hundreds of picoseconds; parent bleach recovery occurs with the same lifetimes. Specifically, the fast-dynamics component has a lifetime of 12 ± 2 ps for **1**, 14 ± 2 ps for **2**, 8 ± 2 ps for **4**, and 12 ± 2 ps for **5** and corresponds to the values typical for vibrational relaxation of excited states. The overall spectral profile decays with a lifetime of 690 ± 15 ps for **1**, 285 ± 9 ps for **2**, 420 ± 6 ps for **5**, and 630 ± 12 ps for **4**, which is attributed to the back electron transfer in the primarily LL′CT excited state to regenerate the ground state.

However, the band at 1564−1575 cm^{-1} exhibits a different behavior, growing in with a lifetime of 10−14 ps and decaying with the same lifetime as that of the longer component of the decays of other transients and of the parent recovery (hundreds of picoseconds). This band is associated with the transiently formed semiquinone unit following formation of the cat → bpy LL′CT excited state and is the low-energy transient, which originated from the ~1600 cm^{-1} ν(CO/CC) catecholate-based vibration of the singlet ground state, as derived from DFT calculations.

The grow-in of this band can be interpreted in one of two ways. The first possibility is that excitation at 400 nm is not selective for the low-energy LL′CT transition but also forms some Pt → diimine MLCT excited state as well (the absorption maximum of the MLCT transition lies in the 400 nm region; see above). Collapse of the higher-lying MLCT state to the lower-lying LL′CT state on a time scale of a few picoseconds would result in the observed grow-in of the sq-based IR transient at ≈1570 cm^{-1}. The 1625 cm^{-1} ν(CO) transient associated with the bpyam ligands in **2** and **5** would not be expected to show the same behavior because relaxation of the MLCT state to the LL′CT state [effectively, a cat → Pt^{III} LMCT process] does not change the electronic structure of the bpyam ligand, which remains as a radical anion in both cases.

Alternatively, grow-in of the sq-based transient at 1570 cm^{-1} could be associated with reorganization of the sq unit immediately after the cat → diimine LL′CT process, associated with vibrational cooling to the structure anticipated in the CT excited state. This would be expected if the structural reorganization required for conversion of a catecholate unit to a semiquinone unit in its equilibrium geometry is particularly large. TA spectra (see the next section) provide some evidence for this, and we note that this rise time correlates well with the 10−14 ps decay process of other transients that are assigned to vibrational cooling.

In either case, the ν(CO/CC) transient band in the 1570 cm^{-1} region, originating from the sq ligand fragment in the excited state, can serve as a marker of the presence of the semiquinoidal form and, moreover, can be used to monitor the dynamics of formation of this form in the course of photoinduced electron transfer and the subsequent structural reorganization.

Ultrafast TA Studies. The dynamics of the excited state in **1** were further investigated by TA spectroscopy, with detection in the 420−760 nm range. Excitation with a 395 nm, ~120 fs pulse resulted in an instantaneous bleach

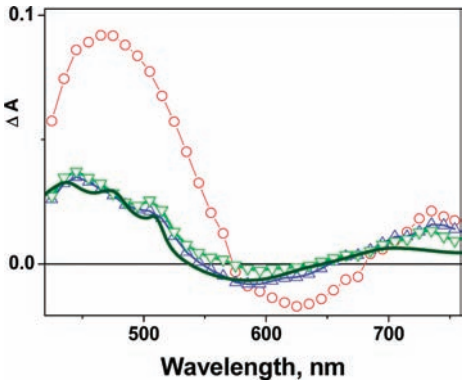

Figure 13. TA spectra of **1** in CH_2Cl_2, obtained following excitation with a 400 nm, ~120 fs laser pulse. The solid line represents a 1:1:1 combination of the absorption spectra of the radical cation and anion and a negative ground-state spectrum of **1**. TA spectra are reconstructed by a global fit with lifetimes of 0.8, 12, and 690 ps (see the text for details) in the A(-○-)→B(-△-)→C(-▽-) model: (○) zero-time spectrum.

of the ground-state LL′CT absorbance at ~600 nm and formation of new transient bands in the visible region. The TA spectrum at zero time, reconstructed through a global fit analysis, shows a broad structureless absorption with a maximum at around 470 nm, interpreted as a local CT excited state. The first excited state evolves with a lifetime of ca. 0.8 ps into the second excited state, the spectrum of which is slightly structured and can be very well approximated by the sum of the absorption spectra of the radical cation and anion and a negative ground-state spectrum taken in a 1:1:1 ratio based on their extinction coefficients (solid line, Figure 13). The second excited state undergoes very minor spectral changes with a lifetime of 12 ps, forming the final spectrum, which then decays with a ca. 690 ps lifetime. Thus, TA data confirm the presence of the radical cation and anion features in the lowest electronic excited state of **1** and show the same three-component dynamics as that observed in the TRIR spectra.

Significantly, the presence in the TA spectrum after just 1 ps of a feature clearly ascribable to a sq fragment (460 and 480 nm) implies that the cat → diimine LL′CT state is formed effectively instantaneously and there is no slow conversion of an initially generated Pt → diimine MLCT state to the LL′CT state. Thus, the ≈10−14 ps grow-in of the TRIR transient band at ≈1570 cm^{-1}, associated with formation of the sq fragment, likely arises from slow vibrational cooling of the LL′CT state associated with a substantial geometric reorganization of the dioxolene fragment after electron transfer (see the previous section).

DFT Calculations. In order to elucidate the nature of the frontier orbitals of the mono- and binuclear complexes and to help in the understanding of the vibrational and electronic spectra of the complexes, DFT calculations were performed on the mononuclear complexes **4** and **6**, dinuclear complex **1**, and also the model dinuclear complex [{Pt(bpy)}$_2$(biscat)] **1′** (analogous to **1** but with no ^{t}Bu substituents on the bpy ligands for computational simplicity).

Geometry optimization for the mononuclear compounds was done using the X-ray data for **3** and **6** as a starting point. For [{Pt(bpy)}$_2$(biscat)], geometry optimization was performed as described in the Experimental Section. The dihedral angle between the two catecholate rings is calculated as 32° in the singlet ground state, in accordance with the behavior of biphenyl-type units in general.[58,59]

The lowest triplet LL′CT excited states of **1′** (denoted as [**1′**]*) and also its one-electron-oxidized radical cation [**1′**]$^{\bullet+}$ show structures very similar to one another with a 19° twist between the halves of the central ligand. This similarity in structure is not surprising given that the CT triplet state can be envisaged as a combination of the complex radical cation with an excess of electron density on one of the bipyridyl ligands. Importantly, the singlet ground state, triplet excited state, and radical-cation state all have a flat structure as a transition state for rotation around the central C−C bond; this flat geometry with a 0° dihedral angle was found to be a saddle point by frequency analysis. The rotation barrier calculated as $E_{twist} - E_{0°}$ is very small: 1.75 kT for the singlet state, 0.45 kT for the triplet state, and 0.4 kT for the radical-cation state, implying an effectively free rotation at room temperature in the triplet and cationic states. The flattening of the structure in [**1′**]* and [**1′**]$^{\bullet+}$ compared to **1′**, as shown by both a reduced dihedral twist and a lower barrier for adoption of a flat structure in the bridging ligand, is significant because it will facilitate electronic delocalization between the halves of the monooxidized (sq/cat) ligand, in agreement with the UV/vis spectroelectrochemical data for **1** (see earlier), which indicate a fully delocalized structure for the monooxidized sq/cat form of the bridging ligand.

With respect to the calculated electronic spectra of **1′**, the calculations show that, in the singlet ground state, the HOMO is indeed delocalized over the entire bridging ligand (see the Supporting Information), while the LUMO is localized principally on the terminal bpy ligand with some Pt contribution. Thus, DFT calculations confirm the CT nature of the lowest excited state in the biscatecholate complex.

Time-dependent DFT (TD-DFT) calculations of the electronic absorption spectrum of [**1′**]$^{\bullet+}$ show excellent agreement with the experimental data (Figure 8); the main transitions are summarized in Table 2, and the key orbitals are shown in Figure 14. The calculations confirm the notion that the intense NIR transition is due to an intra(bridging ligand) transition that is fully delocalized and, therefore, does not have end-to-end cat → sq CT character that would arise in a valence-localized description. This is clearly demonstrated in the pictorial representation of the frontier orbitals (Figure 14 and Supporting Information). The transition at 770 nm is, therefore, a LL′CT process originating from the monooxidized sq/cat bridging ligand to the diimine π^*. The high-energy shoulder at ca. 1200 nm on the main NIR transition may plausibly be ascribed to a vibrational fine structure because it is not accounted for by the DFT calculations of the electronic transition and is 1000 cm^{-1} away from the peak maximum, which is a value typical of a skeletal vibration for an aromatic ligand.

In the triplet excited state [**1′**]*, the HOMO (which is a SOMO originating from the LUMO of the ground state) is clearly localized on the bipyridine, as is the LUMO (Figure 15). Importantly, the first (triplet) excited state from this lowest triplet state (obtained via a TD-DFT

Table 2. Electronic Spectrum for the Cationic Species $\{Pt(bpy)\}_2(biscat)^{\bullet+}$ [a]

no.	energy (cm^{-1})	wavelength (nm)	oscillator strength	major contributions
1	7 186	1391	0.366	HOMO(β) → LUMO(β) (73%)
5	12 970	771	0.210	HOMO(α) → LUMO(α) (31%), HOMO(β) → L+2(β) (54%)
7	14 264	701	0.193	H-2(β) → LUMO(β) (82%)
41	24 443	409	0.067	H-3(α) → L+1(α) (11%), H-1(α) → L+5(α) (20%)
43	24 550	407	0.123	HOMO(α) → L+8(α) (12%), H-8(β) → LUMO(β) (64%)
50	26 740	374	0.256	HOMO(α) → L+8(α) (40%), H-8(β) → LUMO(β) (10%)

[a] Cut-off on oscillator strengths: 0.04. Total number of states in the calculation: 50.

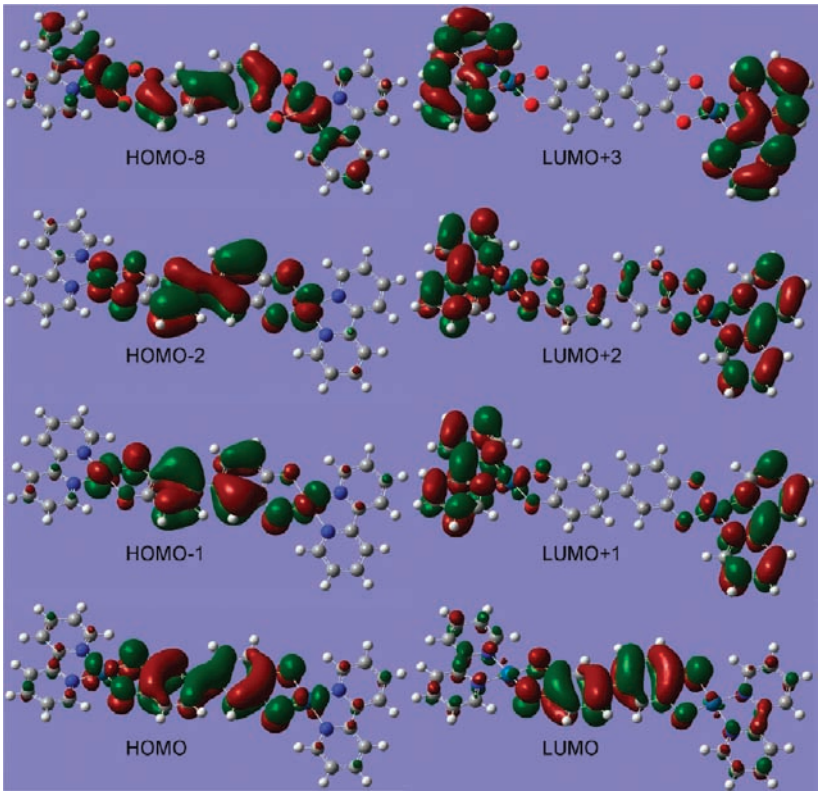

Figure 14. Orbitals involved in the major electronic transitions on the β manifold of the monocation $[\{Pt(bpy)\}_2(biscat)]^{\bullet+}$.

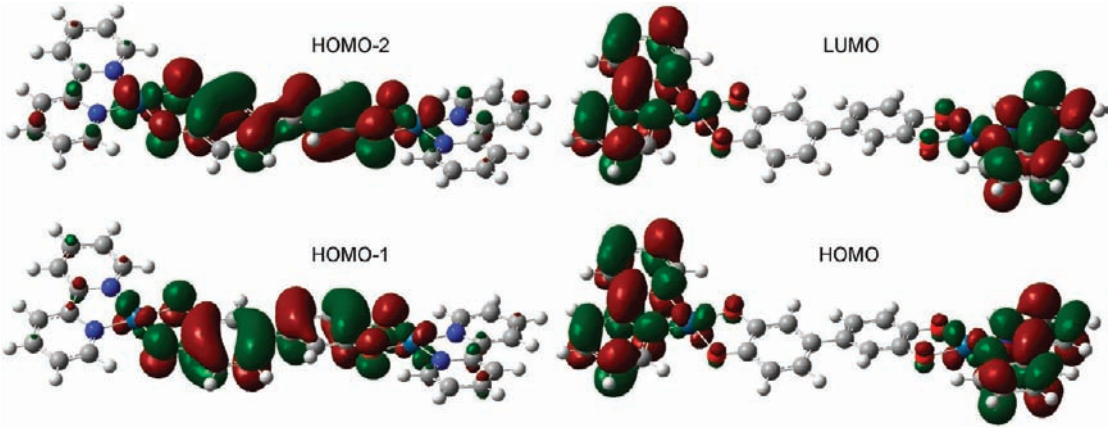

Figure 15. Frontier molecular spin orbitals for the triplet state of the complex $[\{Pt(bpy)\}_2(biscat)]$ (α-manifold). Orbital energies for these orbitals are −0.187 75, −0.171 63, −0.117 87, and −0.111 11 au, respectively.

calculation on [**1′**]*) lies only 0.074 eV higher in energy and is mainly an excitation from HOMO to LUMO, which means that the LUMO and HOMO are near-degenerate. As a result, a linear combination of these will also be a solution of the Schrödinger equation with an energy very similar to the one obtained in our calculations. The HOMO−2 (−5.108 eV) and HOMO−1 (−4.670 eV) are delocalized across the entire bridging ligand (formally

in the sq/cat oxidation level) and are only 3530 cm^{-1} apart in energy. Therefore, in this case, calculations do not clearly predict whether the triplet structure has "localized" or "delocalized" nature with respect to the bridging ligand, but on the basis of the discussion above, we assume that the monooxidized bridging ligand is fully delocalized in [**1′**]*, as it is in [**1′**]$^{\bullet+}$.

Vibrational spectra calculated for the singlet, triplet, and cationic forms match the experimental spectra with scaling factors of 0.98, 0.98, and 0.975, respectively; the detailed data are given in Supporting Information. These data support the presence of the ν(CO/CC) vibration in the cationic and triplet states of mono- and biscatecholate complexes at ca. 1570 cm^{-1} (0.98 scaling factor), which originates from a ca. 1600 cm^{-1} vibration of the singlet ground state that is downshifted when the bridging ligand is oxidized, either transiently (TRIR data) or electrochemically (IR spectroelectrochemistry data).

Conclusions

A series of mono- and dinuclear platinum(II) diimine catecholate complexes have been prepared and extensively studied. A combination of UV/vis absorption, UV/vis/NIR, IR, and EPR spectroelectrochemistry and TA studies, combined with DFT calculations, has provided a complete picture of the behavior of several mononuclear complexes of the type [Pt(cat)(diimine)] in which the lowest excited state is cat → diimine (ligand-to-ligand) CT. For the first time, the structure and dynamics of the LL′CT excited states in {Pt(diimine)(cat)} complexes have been studied by picosecond TRIR spectroscopy and, in the case of **1**, also by femtosecond TA spectroscopy. The excited states show transient IR spectra, which include features characteristic of both bpy ligand radical anions and semiquinone species, in agreement with their LL′CT nature. The TRIR transient spectra decay with two time constants of ca. 10 ps (vibrational cooling) and hundreds of picoseconds (back electron transfer). One particular IR transient associated with the formation of a semiquinone unit grows in on a time scale of ca. 10 ps.

Information obtained from the mononuclear complexes has been used to understand the properties of the (new) dinuclear complexes based on the biscatecholate bridging ligand. These dinuclear complexes show several interesting properties, as follows:

(i) There is a substantial separation between the two successive bridging-ligand-based oxidations, indicative of an intermediate "cat/sq" state that is strongly delocalized; UV/vis/NIR spectroelectrochemistry confirms this, showing a relatively narrow, intense, and low-energy IVCT transition (1425 nm, ε 19 100 L mol^{-1} cm^{-1}) that is a $\pi-\pi^*$ transition delocalized over the bridging ligand. DFT calculations support this, showing that the monooxidized cat/sq form of the bridging ligand can adopt a near-planar conformation with fully delocalized frontier orbitals.

(ii) Aggregation in solution in one case (complex **2**) results in two "half-electron" transfers for the second ligand-based oxidation (sq/cat → sq/sq) of a dinuclear complex.

(iii) In the LL′CT excited state, the transiently oxidized bridging ligand (formally in the cat/sq state) is also likely to be fully delocalized over both rings of the bridging ligand because it is in the chemically oxidized state, whereas the reduced diimine ligand is localized at one terminus of the complex.

Thus, this paper describes the most detailed analysis of the ground- and excited-state electronic structures and the first study of excited-state dynamics, with the use of ultrafast IR and UV/vis TA techniques, of platinum(II) diimine mono- and biscatecholate complexes. It notes the overwhelmingly strong NIR absorption of the one-electron-oxidized binuclear complexes and identifies an IR band in the fingerprint region that could serve as a marker for following the dynamics of formation/decay of the semiquinoidal structure in the oxidized state and in the excited state of both mono- and binuclear platinum(II) chromophores, with the properties underpinning the rich electrochemical and photochemical behavior of this class of complexes.

Experimental Section

Synthesis. All starting materials were obtained from commercial sources and used without further purification. 3,3′,4,4′-Tetrahydroxybiphenyl (H_4biscat)[6,88] and Pt(DMSO)$_2$Cl$_2$ were prepared according to the literature methods; Pt(diimine)Cl$_2$ complexes were prepared as previously described,[56] from Pt(DMSO)$_2$Cl$_2$ and the corresponding diimine ligand, and purified by column chromatography using CH_2Cl_2/MeOH on silica.

Synthesis of Platinum(II) Complexes. Mononuclear {Pt(cat)(diimine)} complexes **3**−**5** were prepared following the general procedure described herein. A mixture of the appropriate Pt(diimine)Cl$_2$, 3,5-di-*tert*-butylcatechol, and ^{t}BuOK in a 1:1:2 molar ratio was stirred at 50 °C in degassed CH_3OH (25 mL) for 20 h under nitrogen. The reaction mixture was cooled to room temperature and diluted with hexane (50 mL or more) to give a dark precipitate, which was filtered and washed with hexane. The product was purified by column chromatography on silica using 2% of CH_3OH in CH_2Cl_2. A minor red impurity was removed, followed by the major blue fraction. This fraction was reduced in volume, and the product precipitated by the addition of hexane.

Pt(bpy)(Bu$_2$cat) (3). A green-yellow solution of ^{t}BuOK (40 mg, 0.36 mmol) and 3,5-di-*tert*-butylcatechol (124 mg, 0.56 mmol) in dry CH_3OH (20 mL) was transferred to a solution of Pt(bpy)Cl$_2$ (211 mg, 0.50 mmol) in dry CH_3OH (20 mL) and the mixture stirred at 50 °C for 20 h in an inert atmosphere. The resultant purple solid that formed was filtered. Purification by column chromatography (SiO_2, 1.75% CH_3OH in CH_2Cl_2) gave a deep-blue fraction that was reduced in volume and precipitated by the addition of hexane. The precipitate was filtered and washed with hexane before being dried in vacuo. Yield: 68 mg, 0.12 mmol (24%). Calculated (found) for $PtC_{24}H_{28}N_2O_2$ $(CH_2Cl_2)_{0.25}$: C, 49.13 (49.18); H, 4.85 (4.67); N, 4.73 (4.72). MALDI-TOF MS [$PtC_{24}H_{28}N_2O_2$ (MW 571.57 g mol^{-1})]: m/z 571. ^{1}H NMR (DMSO-d_6): δ 1.21 (s, 9H), 1.46 (s, 9H), 6.26 (d, J = 1.2 Hz, 1H), 6.46 (d, J = 1.3 Hz, 1H), 7.75 (t, J = 6.82 Hz, 1H), 7.86 (t, J = 6.82 Hz, 1H), 8.36 (dt, J = 4.6 and 7.9 Hz, 2H), 8.54 (d, J = 8.34 Hz, 2H), 9.19 (t, J = 6.22 Hz, 2H). We note that in acetone-d_6 the signal at 9.19 ppm appears as a pair of doublets.

Pt(^{t}Bu$_2$bpy)(Bu$_2$cat) (4). A mixture of 3,5-di-*tert*-butylcatechol (85 mg, 0.38 mmol) and ^{t}BuOK (88 mg, 0.79 mmol) was degassed, and MeOH (20 mL) added. The solution was stirred for 80 min before Pt(^{t}Bu$_2$bpy)Cl$_2$ (201 mg, 0.38 mmol) was added. The reaction mixture was refluxed at 70 °C under an inert atmosphere for 19 h. The solvent was removed, and then the product was redissolved in CH_2Cl_2 and purified on a silica column with 0.25−0.5% MeOH in CH_2Cl_2. Yield: 167 mg, 0.24 mmol (64%). The NMR and elemental analysis data are

(88) Iyoda, M.; Otsuka, H.; Sato, K.; Nisato, N.; Oda, M. *Bull. Chem. Soc. Jpn.* **1990**, *63*, 80–87.

consistent with those reported previously.[56] IR (Nujol mull): 534, 598, 640, 724, 755, 826, 844, 903, 981, 1025, 1120, 1158, 1201, 1240, 1288, 1316, 1367, 1415, 1439, 1468, 1560, 1620 cm^{-1}.

Pt(bpyam)(Bu_2cat) (5). Pt(bpyam)(Bu_2cat) (150 mg, 0.24 mmol) and 3,5-di-*tert*-butylcatechol (55 mg, 0.24 mmol) were added to CH_3OH (30 mL). ^{t}BuOK (54 mg, 0.49 mmol) was added, and the solution was stirred at 70 °C for 20 h in an inert atmosphere. The dark-blue solution was reduced and purified by column chromatography (SiO_2, 1.5% CH_3OH in CH_2Cl_2). The blue fraction eluted was precipitated by the addition of hexane. The precipitate was filtered and dried in vacuo. Yield: 68 mg, 0.09 mmol (37%)

Calcd for $PtC_{34}H_{46}N_4O_4$ (MW 769.83 g mol^{-1}): C, 53.05; H, 6.02; N, 7.28. Found: C, 51.65; H, 6.05; N, 7.02. Calcd for $PtC_{34}H_{46}N_4O_4(CH_2Cl_2)_{0.3}$: C, 51.80; H, 5.91; N, 7.04. MALDI-TOF MS: m/z 769. ^{1}H NMR (DMSO-d_6): δ 1.09 (dt, J = 2.4 and 7.1 Hz, 6H), 1.18−1.24 (m, 15H), 1.46 (s, 9H), 3.24 (q, J = 7.0 Hz, 4H), 3.50 (q, J = 7.1 Hz, 4H), 6.27 (d, J = 2.2 Hz, 1H), 6.48 (d, J = 2.2 Hz, 1H), 7.72 (dd, J = 1.7 and 5.8 Hz, 1H), 7.85 (dd, J = 1.6 and 5.8 Hz, 1H), 8.69 (t, J = 1.7 Hz, 2H), 9.23 (dd, J = 3.4 and 5.9 Hz, 2H). IR (Nujol mull): 551, 587, 639, 727, 755, 810, 850, 915, 946, 978, 1024, 1066, 1104, 1216, 1240, 1285, 1316, 1360, 1385, 1414, 1443, 1456, 1472, 1540, 1560, 1634 cm^{-1}.

Pt(dppe)(Bu_2cat) (6). A mixture of 3,5-di-*tert*-butylcatechol (49 mg, 0.22 mmol) and ^{t}BuOK (51 mg, 0.46 mmol) was degassed, and degassed MeOH (30 mL) was added. The mixture was stirred for 50 min before Pt(dppe)Cl_2 (153 mg, 0.23 mmol) was added, and the reaction was heated to 50 °C under nitrogen for 2 h. The mixture was cooled and reduced in volume, and the product was precipitated by the addition of hexane. The product was filtered, washed with hexane, and dried under vacuum. Yield: 33 mg, 0.04 mmol (18%). ^{1}H NMR ($CDCl_3$): δ 1.33 (s, 9H), 1.40 (s, 9H), 2.34−2.53 (m, 4H), 6.61 (d, J = 2.21 Hz, 1H), 6.94 (d, J = 2.27 Hz, 1H), 7.34−7.46 (m, 12H), 8.02−8.10 (m, 4H), 8.12−8.19 (m, 4H). ^{31}P NMR: δ 32.11, 31.99, 30.43, and 30.31. Pt satellites: δ 48.82, 47.11, 15.17, and 13.76. $J(^{31}P-^{195}Pt)$: 3403 Hz. Calcd for $PtC_{40}H_{44}P_2O_2(CH_2Cl_2)_{0.25}$ (found): C, 57.89 (57.76); H, 5.37 (5.25). ES^+ MS. Calcd for $PtC_{40}H_{44}P_2O_2$: 813.80 g mol^{-1}. Found: 814 g mol^{-1} ($M - H^+$). IR (Nujol mull): 535, 573, 617, 651, 668, 692, 714, 748, 809, 877, 976, 1027, 1105, 1193, 1241, 1281, 1321, 1354, 1386, 1411, 1436, 1456, 1472, 1505, 1557, 1575 cm^{-1}.

Dinuclear Complexes 1 and 2, (Pt(diimine))$_2$(biscat). A mixture of tetrahydroxybiphenyl and ^{t}BuOK in a 1:4 molar ratio was stirred in degassed CH_3OH for 40 min. A total of 2 equiv of the appropriate Pt(diimine)Cl_2 was added and then stirred at 70 °C for 20 h under nitrogen. The reaction mixture was cooled to room temperature, and the resulting precipitate was filtered. The product was purified on silica using 2.5% CH_3OH in CH_2Cl_2 as the eluent. A minor yellow impurity was removed, followed by the major blue fraction. This fraction was reduced in volume and precipitated by the addition of hexane (minimum of 50 mL).

{Pt(^{t}Bu_2bpy)}$_2$(biscat) (1). A mixture of tetrahydroxybiphenyl (52 mg, 0.24 mmol) and ^{t}BuOK (88 mg, 0.79 mmol) was stirred in CH_3OH for 40 min. Pt(^{t}Bu_2bpy)Cl_2 (199 mg, 0.37 mmol) was added, and the solution was stirred at 70 °C for 20 h in an inert atmosphere. The product was filtered and purified by column chromatography (SiO_2, 2.5% CH_3OH in CH_2Cl_2). The deep blue fraction was reduced in volume and precipitated by the addition of hexane. The precipitate was filtered and dried in vacuo. Yield: 70 mg, 0.06 mmol (32%). Calcd for $Pt_2C_{48}H_{54}N_4O_4(CH_2Cl_2)_{0.25}$ (found): C, 48.86 (49.59); H, 4.73 (4.97); N, 4.82 (5.13). MALDI-TOF MS [$Pt_2C_{48}H_{54}N_4O_4$ (MW 1141.12 g mol^{-1})]: m/z 1141.

IR (Nujol mull): 559, 598, 652, 736, 802, 850, 878, 903, 1020, 1079, 1124, 1158, 1201, 1254, 1370, 1421, 1474, 1541, 1567, 1619 cm^{-1}.

{Pt(bpyam)}$_2$(biscat) (2). A mixture of tetrahydroxybiphenyl (21 mg, 0.1 mmol) and ^{t}BuOK (43 mg, 0.38 mmol) was stirred in CH_3OH for 40 min. Pt(bpyam)Cl_2 (120 mg, 0.19 mmol) was added, and the solution was stirred at 70 °C for 20 h in an inert atmosphere, resulting in precipitation of the product. The product was filtered and purified by column chromatography (SiO_2, 2.5% CH_3OH in CH_2Cl_2). The deep-blue fraction was reduced in volume and precipitated by the addition of hexane. The precipitate was filtered and dried in vacuo. Yield: 50 mg, 0.04 mmol (42%). MALDI-TOF MS [$Pt_2C_{52}H_{58}N_8O_8$ (MW 1313.22 g mol^{-1})]: m/z 1312 ($M - H^+$). ^{1}H NMR (DMSO-d_6): δ 1.09 (t, J = 6.9 Hz, 12H), 1.21 (t, J = 6.8 Hz, 12H), 3.24 (q, J = 7.4 Hz, 8H), 3.51 (q, J = 6.7 Hz, 8H), 6.41−6.56 (m, 4H), 6.71 (d, J = 1.6 Hz, 2H), 7.74 (t, J = 5.5 Hz, 4H), 8.70 (d, J = 1.32 Hz, 4H), 9.23 (dd, J = 3.5 and 5.8 Hz, 4H).

Materials and Equipment. CV was carried out using an Autolab potentiostat 100 controlled by a PC running software *GPES*, version 4.9. The working electrode was a platinum disk, the counter electrode a piece of platinum wire, and the reference Ag^+/AgCl.

UV/vis spectroscopy studies were carried out using a Cary 50 Bio controlled by a PC running Cary WinUV Scan Application, version 3.00.

IR spectroelectrochemistry was performed using a Perkin-Elmer FTIR spectrophotometer controlled by a PC running Perkin-Elmer's own software *Spectrum*, version 3.02.

The optically transparent thin-layer electrochemical (OTTLE) cell used was similar to that used by Hartl et al. UV/vis/NIR spectroelectrochemistry experiments were conducted using a Cary 5000 spectrophotometer controlled by a PC running WinUV Scan Application, version 3.00. An OTTLE cell was used. The working electrode was platinum gauze in the path of the beam, the counter electrode was platinum wire, and silver wire was used as the reference electrode. The potentiostat used was EG&G Applied Research potentiostat/galvanostat model 273A.

EPR spectra were recorded on a Bruker EMX spectrometer fitted with a frequency counter. Spectral simulations were accomplished using WINEPR SimFonia version 1.25 (Bruker Analytische Messtechnik GmbH).

X-ray Diffraction. Data were collected on a Bruker Smart CCD area detector with an Oxford Cryosystems low-temperature system. Reflections were measured from a hemisphere of data collected of frames, each covering ω = 0.3°. All reflections were corrected for Lorentz and polarization effects and for absorption by semiempirical methods based on symmetry-equivalent and repeated reflections. The structure was solved by direct methods and refined by full-matrix least-squares methods on F^2. Complex scattering factors were taken from the program package *SHELXTL*,[89] as implemented on an IBM PC. Hydrogen atoms were placed geometrically and refined with a riding model (including torsional freedom for methyl groups) and with U_{iso} constrained to be 1.2 (1.5 for methyl groups) times U_{eq} of the carrier atom. Data in common: T = 150(2) K, λ = 0.710 73 Å. Complex scattering factors were taken from the program package *SHELXTL*,[89] as implemented on the Viglen Pentium computer.

Crystal data for $C_{24}H_{28}N_2O_2Pt$ (**3**): M = 571.57 g mol^{-1}. **3** crystallizes by the slow diffusion of hexane in a dichloromethane solution as purple plates; crystal dimensions 0.26 × 0.12 × 0.01 mm^3; monoclinic, a = 13.6241(10) Å, b = 11.8742(9) Å, c = 13.5310(10) Å, β = 90.795(3)°, U = 2188.8(3) Å^3, Z = 4, D_c = 1.735 Mg m^{-3}, space group $P2_1/c$, Mo Kα radiation ($\bar{\lambda}$ = 0.710 73 Å), μ(Mo Kα) = 6.432 mm^{-1}, F(000) = 1120. Refinement converged at a final R1 = 0.0160 (wR2 = 0.037 59, for all 6693 data, 268 parameters, mean and maximum δ/σ 0.000, 0.004) with allowance for the thermal anisotropy of all

(89) Sheldrick, G. M. *Acta Crystallogr.* **2008**, *A64*, 112–122.

non-hydrogen atoms. Minimum and maximum final electron densities −0.555 and 1.937 e Å^{-3} (the latter being 0.84 Å from Pt1). A weighting scheme $w = 1/[\sigma^2(F_o^2) + (0.176P)^2 + 1.3135P]$, where $P = (F_o^2 + 2F_c^2)/3$ was used in the latter stages of refinement.

Crystal data for $C_{41}H_{45}Cl_3O_2P_2Pt$ (**6**); $M = 933.25$ g mol^{-1}. **6** crystallizes from chloroform as yellow blocks; crystal dimensions $0.35 \times 0.25 \times 0.25$ mm^3; monoclinic, $a = 12.948(5)$ Å, $b = 28.783(5)$ Å, $c = 24.459(5)$ Å, $\beta = 95.743(5)°$, $U = 9070(4)$ Å^3, $Z = 4$, $D_c = 1.367$ Mg m^{-3}, space group $P2_1/c$, Mo Kα radiation ($\lambda = 0.710\,73$ Å), μ(Mo Kα) = 3.371 mm^{-1}, $F(000) = 3728$. Refinement converged at a final R1 = 0.0413 (wR2 = 0.0905, for all 20 719 data, 895 parameters, mean and maximum δ/σ 0.000, 0.000) with allowance for the thermal anisotropy of all non-hydrogen atoms. Minimum and maximum final electron densities −0.887 and 1.880 e Å^{-3}. A weighting scheme $w = 1/[\sigma^2(F_o^2) + (0.0326P)^2 + 0.2593P]$, where $P = (F_o^2 + 2F_c^2)/3$ was used in the latter stages of refinement.

DFT Calculations. All of our calculations were performed using the SMP version of *Gaussian 03*[90] using the B3LYP functional method.[91] Gaussian was compiled using the Portland Compiler 8.0-6 with the Gaussian-supplied version of BLAS on the EMT64 architecture. In all calculations, we used a Stuttgart/Dresden pseudopotential on platinum atoms and the D95 V basis set on all other atoms.[92−94] No solvent effects were included in the calculations. The neutral complex (284 electrons and 487 basis functions) was treated as a singlet, whereas the cation was assumed to be a doublet. All optimizations were performed using ultrafine integrals because, in our experience, this aids convergence. No symmetry was taken into account in our calculations. On the basis of the optimized structures, we calculated the UV/vis spectra of each compound using a single-point TD-DFT[95−97] calculation using tight self-consistent-field convergence criteria. In each calculation, we calculated at least 50 transitions. The electronic and vibrational spectra were analyzed using the *Gaussum* program.[98]

Our computational procedure was as follows. First, we optimized the neutral complex starting from the crystal structure. From the optimized geometry, we calculated frequencies in the harmonic approximation. Because it is well-known that B3LYP overestimates frequencies, these were scaled by 0.98 to obtain better agreement with the experiment. For the biscatechol-based species, we ran calculations both from a flat and from a bent structure to obtain energies for both. Frequencies were obtained in the usual way. However, for the triplet state, the analytical frequency calculation did not converge and we were forced to obtain them numerically using the option freq = numer.

Obtaining the correlations between the vibrations of the neutral and cationic complexes can be quite a daunting task, if done purely visually, if only because of the large number of vibrations for these complexes. So, to avoid any problems, we used a mixed approach. We recognize that the displacement vectors, printed by *Gaussian*, form an orthonormal set. Additionally, the moments of inertia do not change significantly between the two species. This means that the displacement vectors for both species are expressed in the same coordinate frame, which means they can be compared without any additional transformations. Thus, to obtain the correlations between the vibrations of the neutral and cationic complexes, we calculated the overlap between the displacement vectors for the two species by taking the inner product over each of the Cartesian coordinates separately and summing over the result. An overlap of 0.7 or better was considered to be a strong correlation. After the correlations were identified numerically, they were checked by visual inspection.

TRIR Spectroscopy. The picosecond TRIR studies were performed on the PIRATE setup in the Rutherford Appleton Laboratory, the details of which are described elsewhere.[71] Briefly, part of the output from a 1 kHz, 800 nm, 150 fs, 2 mJ titanium sapphire oscillator/regenerative amplifier was used to pump a white-light continuum seeded BBO optical parametric amplifier (OPA). The signal and idler produced by this OPA were difference frequency mixed in a type I $AgGaS_2$ crystal to generate tunable mid-IR pulses (ca. 150 cm^{-1} bandwidth). Second-harmonic generation of the residual 800-nm light provided 400-nm pulses, which were used to excite the sample. Probe and pump beam diameters in the sample were around 100 and 150 μm, respectively, and the pump energy in the sample was 3−4 μJ. Changes in IR absorption were recorded by normalization of the outputs from a pair of 64-element HgCdTe linear-IR array detectors on a shot-by-shot basis. Gratings of 300 lines mm^{-1} were used in the spectrographs to achieve a high spectral resolution (approximately 4 cm^{-1}).

The studies of **1** and **4** were conducted on an ULTRA[99] facility, a cluster of sensitive ultrafast IR and Raman spectrometers. The IR spectrometer used comprised two synchronized 10 kHz, 8 W, 40 fs and 2 ps titanium sapphire oscillator/regenerative amplifiers (Thales). These pump a range of OPAs. A portion of the 40 fs Ti:Sapph beam was used to generate a tunable mid-IR probe light with around a 400 cm^{-1} bandwidth. The 400 nm pump beam was generated from the second harmonic of the 40 fs laser. Probe and pump beam diameters in the sample were around 70 and 120 μm, respectively, and the pump energy in the sample was around 1−1.5 μJ. In this case, changes in the IR absorption spectra were recorded by three HgCdTe linear-IR array detectors on a shot-by-shot basis. Two 128 element arrays were used to collect spectra in the 1200−1700 cm^{-1} range (approximately 4 cm^{-1} resolution), and one 64-element array acted as a reference. All experiments were carried out in Harrick cells with 2-mm-thick CaF_2 windows with 500−950 μm sample path lengths and a typical optical density of 0.5−1 at 400 nm. All samples were rastered and flowed.

Picosecond TA. Experiments were performed at the B. I. Stepanov Institute of Physics, Minsk, Belarus, on a pump−probe spectrometer based on a homemade original femtosecond

(90) Frisch, M. J.; T., G. W.; Schlegel, H. B; Scuseria, G. E.; Robb, M. A.; Cheeseman, J. R.; Montgomery, J. A., Jr.; Vreven, T.; Kudin, K. N.; Burant, J. C.; Millam, J. M.; Iyengar, S. S.; Tomasi, J.; Barone, V.; Mennucci, B.; Cossi, M.; Scalmani, G.; Rega, N.; Petersson, G. A.; Nakatsuji, H.; Hada, M.; Ehara, M.; Toyota, K.; Fukuda, R.; Hasegawa, J.; Ishida, M.; Nakajima, T.; Honda, Y.; Kitao, O.; Nakai, H.; Klene, M.; Li, X.; Knox, J. E.; Hratchian, H. P.; Cross, J. B.; Bakken, V.; Adamo, C.; Jaramillo, J.; Gomperts, R.; Stratmann, R. E.; Yazyev, O.; Austin, A. J.; Cammi, R.; Pomelli, C.; Ochterski, J. W.; Ayala, P. Y.; Morokuma, K.; Voth, G. A.; Salvador, P.; Dannenberg, J. J.; Zakrzewski, V. G.; Dapprich, S.; Daniels, A. D.; Strain, M. C.; Farkas, O.; Malick, D. K.; Rabuck, A. D.; Raghavachari, K.; Foresman, J. B.; Ortiz, J. V.; Cui, Q.; Baboul, A. G.; Clifford, S.; Cioslowski, J.; Stefanov, B. B.; Liu, G.; Liashenko, A.; Piskorz, P.; Komaromi, I.; Martin, R. L.; Fox, D. J.; Keith, T.; M. A. Al-Laham, Peng, C. Y.; Nanayakkara, A.; Challacombe, M.; Gill, P. M. W.; Johnson, B.; Chen, W.; Wong, M. W.; Gonzalez, C.; Pople, J. A. *Gaussian 03*, revision C.02; Gaussian, Inc.: Wallingford, CT, 2004.

(91) Becke, A. D. *J. Chem. Phys.* **1993**, *98*, 5648.

(92) Nicklass, A.; Dolg, M.; Stoll, H.; Preuss, H. *J. Chem. Phys.* **1995**, *102*, 8942–8952.

(93) Cao, X. Y.; Dolg, M. *J. Chem. Phys.* **2001**, *115*, 7348–7355 and references cited therein.

(94) Dunning, T. H., Jr.; Hay, P. J. In *Modern Theoretical Chemistry*; Schaefer, H. F., III, Ed.; Plenum: New York, 1976; Vol. *3*, pp 1−28.

(95) Strattmann, R. E.; Scuseria, G. E.; Frisch, M. J. *J. Phys. Chem.* **1998**, *109*, 8218–8224.

(96) Bauernschmidt, R.; Ahlrichs, R. *Chem. Phys. Lett.* **1996**, *256*, 454.

(97) Casida, M. E.; Jamorski, C.; Casida, K. C.; Salahub, D. R. *J. Chem. Phys.* **1998**, *108*, 4439–4449.

(98) O'Boyle, N. M.; Tenderholt, A. L.; Langner, K. M. *J. Comput. Chem.* **2008**, *29*, 839.

(99) Kania, R.; Stewart, A. I.; Clark, I. P.; Greetham, G. M.; Parker, A. W.; Towrie, M.; Hunt, N. T. *Phys. Chem. Chem. Phys.* **2010**, *12*, 1051–1063.

Ti:Sapph pulsed oscillator and regenerative amplifier system operated at 10 Hz repetition rate.[100] A Ti:Sapph master oscillator was synchronously pumped with the doubled output of a homemade mode-locked picosecond pulsed Nd:YAG laser. The regenerative amplifier was pumped with nanosecond Q-switched Nd:YAG laser LS-2134 (LOTIS TII). The pulse width and energy of the Ti:Sapph system after the amplifier were ca. 150 fs and 0.5 mJ, respectively, tunable over the spectral range 760−820 nm. The fundamental output of the Ti:Sapph system (a 790 nm output wavelength was set for the present study) was split into two beams in the ratio 1:4. The more intense beam was passed through a controlled delay line and, after frequency doubling (to provide 395 nm radiation), was utilized for sample pumping. The energy of 395 nm pump pulses was ca. 40 μJ, being focused to a 500 × 500 μm spot on the sample. The second beam of the fundamental frequency was used for the generation of a femtosecond supercontinuum (by focusing into a 1-cm-path-length cell with water), which served as the probe radiation. The continuum probe light was split with a beam splitter into two pulses (reference and signal), identical in intensity, and the signal was focused on the sample by mirror optics. The spectra of both pulses were recorded for each laser flash by a polychromator equipped with a CCD camera and transferred to the computer. The time resolution of the setup is limited by the pump and probe pulse duration and estimated as ca. 0.2 ps. A solution of studied compounds in CH_2Cl_2 in a 5-mm quartz cell was bubbled with argon prior to the experiments, and the positive pressure of the inert gas was maintained over the course of the experiment.

(100) Blokhin, A. P.; Gelin, M. F.; Buganov, O. V.; Dubovskii, V. A.; Tikhomirov, S. A.; Tolstorozhev, G. B. *J. Appl. Spectrosc.* **2003**, *70*, 70–78.

Acknowledgment. We thank the EPSRC (J.A.W.), Centre for Molecular Structure and Dynamics of STFC and EPSRC for the CASE award (J.A.W. for J.B.), Marie Curie Incoming International Fellowship (I.V.S), Royal Society, STFC for the award of beam time, and University of Sheffield for support. We are also grateful to Dr. T. Easun for providing some of the bpyam ligand, F. Piccinelli for assistance with some of the syntheses, and Prof B. T. Pickup for fruitful discussions. All calculations were run at the Jupiter Cluster of the Theoretical Chemistry Group of the University of Sheffield.

Supporting Information Available: X-ray crystallographic data in CIF format (CCDC 792165 for compound **3**, and CCDC 792166 for compound **6**), additional absorption spectra, TRIR data, spectroelectrochemical data, crystallographic data, details of the calculated structures, anisotropic thermal vibrational parameters with esd's, hydrogen-atom position parameters, observed structure amplitudes, and calculated structure factors. This material is available free of charge via the Internet at http://pubs.acs.org.